Effects of Machining on the Uniaxial and Equibiaxial Flexure Strength of CAP3 AD-995 Al_2O_3

Andrew A. Wereszczak,[1] Jeffrey J. Swab, and Reuben H. Kraft[2]
Metals and Ceramics Research Branch
Weapons and Materials Research Directorate
Aberdeen Proving Ground, MD 21005

ARL Technical Report
October 2003

[1] Presently with the Ceramic Science and Technology Group, Metals and Ceramics Division, Oak Ridge National Laboratory, Oak Ridge, TN, wereszczakaa@ornl.gov.

[2] ORISE Student in Mechanical Engineering Department, University of Maryland - Baltimore County at the time this work was performed. Presently pursuing graduate studies in the Mechanical Engineering Department, Johns Hopkins University, Baltimore, MD.

Table of Contents

Executive Summary

The effect of surface condition on the uniaxial and equibiaxial flexure strength of CoorsTek's CAP3 AD-995 alumina was examined. Note that this material was found *not* to be the same as CoorsTek's AD-995 alumina - a comparison and discussion of their differences are provided in this report. The following four surface conditions were considered with the CAP3 AD-995: as-fired (i.e., unmachined) surfaces; the surface condition produced by CoorsTek's standard surface grinding procedures (i.e., the surface condition they will provide on tiles unless otherwise specified); the surface condition resulting from uniaxial surface grinding with 320-grit diamond machining (i.e., that surface machining method specified for ASTM C1161-94 ceramic flexure bars), and rotary surface grinding with 320-grit diamond machining.

CoorsTek manufactures and markets two grades of compositionally equivalent, 99.5%-purity alumina, designated by CoorsTek as "AD-995" and "CAP3 AD-995"; the latter was tested in the present study. Unfortunately, confusion often results when examining the literature because of that compositional equivalency and because authors tend to often generically report both as "AD-995", so it is difficult (if not impossible) for readers to discern which of the two CoorsTek 99.5% alumina grades was interrogated unless microstructural evaluations were actually performed and reported on. Adding to this confusion is the fact that CoorsTek reports the same average grain size (and other properties too) for these two 99.5% grades (though an average size of 1.5 and 5.7 μm was respectively measured for AD-995 and CAP3 AD-995 in the present study); though their values may be statistically correct, the narrow and wide grain size distributions of the AD-995 and CAP3 AD-995 grades respectively are not illustrated by that mean value. Microstructures for both grades are reported and described to (1) show the differences between these two grades and to (2) promote to possible investigators of either grade of "AD-995" that it behooves them to understand the microstructure of the "AD-995" and to recognize which of the two grades that they are actually investigating. The understanding of their differences is important as the AD-995 alumina is omnipresent in the structural ceramic literature whereas CAP3 AD-995 is somewhat relegated to the armor community (though suspicion exists that AD-995 is actually the 99.5% alumina grade that is often ballistically- or high-strain-rate tested – that suspicion unfortunately cannot be supported nor denied unless grain size distribution information or microstructures accompanied those studies).

There was rationale behind the use of two different flexure tests in this study. Uniaxial flexure strength testing was performed because it is the most common and recognizable strength test for ceramics, and equibiaxial[3] flexure strength testing was conducted because it enabled the strength characterization of a ceramic tile and because it is believed to better mimick (than uniaxial flexure testing) the deflection that results from on-center ballistic loading of armor tiles. Interest existed to link the generated strength distributions from the two flexure test configurations while examining how surface condition affected both.

Both flexure tests utilized established and demonstrated practices. Uniaxial flexure strength testing adhered to ASTM C1161B practices and involved four-point-bending of bars sectioned from tiles that had one of the four surface conditions; that surface condition was oriented to be on the tensile face of the bend specimen and was sampled during uniaxial flexure strength testing. The effect of chamfered (or unchamfered) bend bar edges on uniaxial flexure strength was also examined. Equibiaxial flexure strength testing consisted of concentric ring-on-ring testing of tiles in which the surface condition was oriented to be on the tensile face of the tile specimen during equibiaxial flexure strength testing. The surface area sampled by the equibiaxial flexure testing was more than one order of magnitude larger than that sampled by the uniaxial flexure testing.

Not surprisingly, strength depended on surface condition. Surfaces that were uniaxial or rotary ground using 320-grit diamond machining generated the highest strengths (equibiaxial flexure characteristic strength = 280 MPa) CAP3 AD-995 alumina, followed in descending order of strengths from as-fired surfaces (equibiaxial flexure characteristic strength = 264 MPa), and then strengths from surfaces produced by CoorsTek's standard grinding procedure (equibiaxial flexure characteristic strength = 244 MPa). Those differences in strengths are statistically significant with 95% confidence. These results show that finer surface finishes produced by 320-grit machining can increase flexure strength, and suggest that CoorsTek's standard surface grinding procedure of CAP3 AD-995 tiles is perhaps too aggressive.

[3] There are many types of "biaxial" strength tests. An "equi"-biaxial strength test is a special case of general "biaxial" strength testing where the two principal stresses have the same sign and magnitude in the specimen gage section.

The balancing of the extra cost of machining CAP3 AD-995 alumina and its beneficial effect on strength needs to proceed with caution. First, though CoorsTek's "standard" machining will provide a tile whose dimensions will have stricter tolerances than those of "as-fired" tiles for an extra cost of $14/tile (tile geometry = 4 x 4 x 0.118 in.), that comes at the expense of lower strengths - a 7-8% decrease. The strength of 320-grit machined tiles was 6% and 15% greater than tiles with as-fired surfaces and CoorsTek "standard" ground surfaces, respectively, but that resulted from an additional expense of $45/tile. If desire remains to have CoorsTek perform the surface machining of their CAP3-AD995 alumina tiles, then a requested combination of a less aggressive machining practice and a finer grit grinding wheel should be considered by the customer. Clearly, the 320-grit machining benefits strength; however, the justification of the extra expense for that relatively low amount of strengthening is subjective and will depend on the needs of the end-user.

As expected, chamfering edges on specimens has a beneficial effect on uniaxial flexure strength. *Not* chamfering uniaxial flexure specimens resulted in a strength loss of approximately 4-8% for a given machining condition for CAP3 AD-995 alumina. The reduction in strength correlated with failure consistently being initiated at the edge of these specimens (an occurrence not observed when bend bar edges were chamfered). A lack of edge chamfering inherently has no effect on equibiaxial flexure strength; however, its presence may indeed may be influential as a tile is mechanically loaded closer to one of its edges (and that edge is chamfered versus unchamfered). Chamfering edges in ceramic specimens and components has been long recognized to increase strength; however, in spite of that recognized effect, the study of chamfered or unchamfered edges in the present study was revisited because ceramic tiles still in fact supplied by vendors with unchamferred edges and interest therefore existed to statistically illustrate their detrimental effect on strength.

Uniaxial flexure testing with ASTM C1161B produced strengths that were dependent on machining direction. The directional-dependence on uniaxial flexure strength was a consequence of the interaction between the extent of anistropic machining damage and the relatively large average grain size of CAP3 AD-995 alumina. The directional-dependence on uniaxial flexure strength effect only complicates the general interpretation of flexure strength's dependence on surface condition, whereas equibiaxial flexure testing facilitates surface condition

comparisons because of its "averaging effect" on machining directionality - it is perhaps a better flexure test for assessing flexure strength of armor tiles.

Equibiaxial flexure strengths were ~ 20% less than uniaxial flexure strengths for any of the four investigated surface conditions: this amount correlates well with predicted strength-size-scaling between the two geometries using Weibull theory. Because this failure stress is lower, and probably more representative of on-center ballistic loading of ceramic tiles, its use is (desirably?) conservative and perhaps better suited than the use of uniaxial flexure strength for input in ballistic models that consider such deflections.

The results from this study show that machining practices can be employed to increase flexure strength which can perhaps have beneficial ramifications on ballistic performance when tile thickness is relatively thin. Issues of flexure strength dependence on surface condition are likely to be more relevant as armor tile thicknesses decrease. Bending-induced deflections for a given load (or impact) will increase as tile thickness decreases, and if those deflections are sufficient to cause (tensile stress induced) failure in the ceramic tile, then proactively increasing flexure strength (e.g., performing finer grit diamond machining) in the ceramic tile will lessen the likelihood of its failure for the same load or impact. Ceramic armor thicknesses that tend to be relatively thin (e.g., WC tiles, body armor) will likely be more affected by flexure-strengthening actions (e.g., finer surface finishes, application of passive oxidation layer on SiC ceramics, etc.) than ceramic armor that are relatively thick (e.g., thick ceramic tiles in vehicular armor).

Conceivably the equibiaxial flexure test apparatus and method utilized in the present study may be extended for use as a quality control "proof test" and discriminate stronger tiles from weaker ones. If stronger tiles (i.e., tiles that can withstand greater center-line deflection prior to fracturing) were linkable to better ballistic performance, then this equibiaxial flexure test could be used to filter out and eliminate from consideration those tiles from a population that have low potential for ballistic performance.

List of Figures

List of Tables

1. Introduction

Though the processes of ballistic impact in ceramic tiles are several and convoluted, and often are complicated to deconvolute and interpret, there are some aspects of the impact event that appear to have links to more established interpretations associated with the fracture event in "static" mechanical tests. For example, the fracture pattern in ceramic armor tiles that are on-center ballistically tested often has similarity to that resulting in ceramic specimens that fractured in "static" equibiaxial flexure strength testing. This observation is reasonable when the whole ballistic event is considered as a sum of localized projectile/tile interaction and macro-structural response of the ceramic tile to mechanical loading.

Ceramic "bend-strength" data is often used in ballistic models to predict performance of the ceramic tiles. Unfortunately, the "bend-strength" of ceramics is an enigmatic parameter at best and non-conservative or misleading at worst. It has long been recognized that the (tensile) strength of monolithic ceramics exhibits "strength-size-scaling" (i.e., "weakest-link-in-a-chain" analog). A large ceramic specimen will fail at a lower stress than a smaller specimen of the same material. Strengths of ceramics typically are better represented by a Weibull distribution than a Gaussian distribution, and their relatively wide scatter has resulted in a combined, size-scaling, Weibull function that relates probability of failure to specimen size and applied stress (and stress gradient too). Further complicating this is the fact that the strength of ceramics, when loaded in flexure or when there is a tensile stress on their surface, is susceptible to the nature of surface condition (and of course how much surface area is under tension). Analogous to scratched or scored glass loaded in flexure, ceramics that have been coarsely machined will typically break at lower bend stresses than the same ceramic that was finely machined. Additionally, a coarse or aggressive machining step prior to finish grinding can introduce significant sub-surface damage that will tend to reduce strength - this can be particularly frustrating because the fine surface finish suggests to the end-user that the strength should be relatively high, however, the hidden effects of the coarse machining often still dominate and lessen strength - an effect that is typically not observed until strength tests are performed, or worse yet, when the tile is unpredictably found not to be able to withstand appreciable bending in service. Introducing machining direction as an independent parameter also affects strength (i.e., the uniaxial flexure strength of a ceramic that was machined in the same direction as the applied tensile stress will typically be higher than when it is machined perpendicular to the applied tensile stress … for the

same extent of machining damage). Because of these complications and trends, the use of a reported "bend strength" of a ceramic without knowing how the associated test specimens were prepared or mechanically tested is introducing danger, and is a primary reason why ASTM C1161 [1] was developed to guide those evaluating the "bend strength" of ceramics.

There were several goals sought in the present study. The primary goal was to examine and portray the above-described static "bend strength" issues in a common armor ceramic, CoorsTek's CAP3 AD-995 alumina, so to make their effects of interest, of relevance, and of use to those in ballistic community. A second goal was to assess if and how alternative machining practices could improve flexure strength of this alumina (with a hypothesis that strengthening can manifest itself in improved ballistic performance). Four surface conditions were considered as an independent parameter: as-fired (i.e., unmachined) surfaces; the surface condition produced by CoorsTek's standard surface grinding procedures (i.e., the surface condition they will produce on tiles unless otherwise specified by its customer); the surface condition resulting from uniaxial surface grinding with 320-grit diamond machining (i.e., that surface machining method formerly specified for ASTM C1161-94 ceramic flexure bars), and rotary surface grinding with 320-grit diamond machining. A third goal was to examine these surface conditions and strength-size-scaling effects using two types of flexure tests: uniaxial and equibiaxial flexure. There was rationale for utilizing both. Uniaxial flexure strength testing was performed because it is the most common and recognizable strength test for ceramics, and equibiaxial flexure strength testing was conducted because it samples a much larger surface and volume and because it is believed to better mimick (than uniaxial flexure testing) the deflection that results from on-center ballistic loading of armor tiles. Interest also existed in linking the strength distributions from the two flexure testing configurations while examining how surface condition affected both.

This report first describes the CAP3 AD-995 alumina, the employed mechanical tests and data analysis, and the independent parameters that were explored. Uniaxial and equibiaxial strengths are then reported and linked and examined as a function of the investigated surface conditions. Lastly, their interpretations are described and suggested ramifications on ballistic performance are presented.

2. Experimental Procedures

A description of the CAP3 AD-995 alumina is first presented followed by descriptions of the investigated surface conditions, the utilized flexure testing, and the data and fracture analyses.

2.1. CAP3 AD-995 Al_2O_3 Description

The Class of an alumina per Mil Spec MIL-P-46199 (MR) [2] is associated with its purity. CAP3-AD995 alumina (Al_2O_3) is a Class 4 alumina, whereas the AD-85, AD-94, and AD-995 aluminas listed in Table 1 are Class 1, Class 3, and Class 4, respectively.

CoorsTek reports [3-4] the properties for CAP3 AD-995 alumina that are listed in Table 1, and they are compared against other aluminas they manufacture. Note that CoorsTek reports the exact same property values for their "AD-995" and "CAP3 AD-995" grades; this suggests that they intend the two compositions to be the same (our results show that is not the case for their microstructures). The CAP3 AD-995 has a purity of 99.5%, a density of 3.90 g/cc, a reported flexure strength of 379 MPa, an elastic modulus of 370 GPa, a Poisson's ratio of 0.22, a hardness of 14.1 GPa (Knoop-1kg), and a fracture toughness between 4-5 MPa m. The authors ran numerous tests and determined: average density of the material to be 3.88 g/cc; average elastic modulus to be 377 GPa by impulse excitation of vibration [5] and 381 GPa by pulse-echo [6]; average Poisson's ratio to be 0.236 by impulse excitation of vibration [5], and; an average 1000g Knoop hardness to be 14.9 GPa.

The CoorsTek reported average grain size of 6 μm and a consistent average size of 5.7 μm was measured by the authors (via digital image analysis using a method that was verified to generate equivalent results to the linear intercept method); however, these average values are far from a complete portrayal of the microstructure of this ceramic. It is evident upon inspection of the CAP3 AD-995 microstructure shown in Fig. 1(a)-(b) that the majority of this alumina's volume is in fact occupied by grains that are much larger than 5.7 - 6.0 μm. Polished sections from specimens from randomly seleted tiles were inspected, and this microstructure was consistently observed in all. A polished microstructure of AD-995 is shown in Fig. 2; it is clear that its microstructure is quite different than that of CAP3 AD-995, see Fig. 1(a). Further grain size distribution analysis (of 375 counted grains) of the CAP3 AD-995, see distribution in Fig. 3, showed that 6.6 % of the grains were larger than 15 μm yet occupy 51 % of the volume, and 14 % of the grains are larger than 10 μm yet occupy 70% of the volume. The grain size

distribution of CAP3 AD-995 is much wider than that for AD-995, as also shown in Fig. 3. Because most of the actual grains in CAP3 AD-995 comprise a small volume of the total bulk, this manifests itself into an average grain size that is misleadingly small. Furthermore, CoorsTek reports an average grain size of 6 μm for the AD-995 alumina (see Table 1) whereas the present study measured a much smaller average value of 1.5 μm (166 grains counted). Somewhat hidden in either the CoorsTek or present study measure of AD-995 average grain size is AD-995's much narrower grain size distribution than CAP3 AD-995 alumina. This is a good illustration of how the meaning of an average grain size value can be an incomplete (or even misleading) microstructure descriptor - especially when the distribution about it is relatively wide.

Unfortunately, confusion quite often results from inspection of the literature as AD-995 and CAP3 AD-995 are often generically reported as "AD-995" (unfortunately this confusion is reinforced by CoorsTek reporting the exact same properties for both grades), so it is difficult (if not impossible) for readers to discern (unless microstructural images appear in their text) which of the two CoorsTek 99.5% alumina grades was interrogated when "AD-995" is the only description given. The understanding of the differences between these two "AD-995" aluminas is important as the AD-995 alumina is omnipresent in the structural ceramic literature whereas CAP3 AD-995 is somewhat relegated to the armor community. The authors suspect that the differences between these two "AD-995" alumina are often taken for granted, and that AD-995 is actually the 99.5% alumina grade that is sometimes ballistically- or high-strain-rate tested – that suspicion unfortunately cannot be supported nor denied though, unless grain size distribution information or microstructures accompany any of the results from those studies.

Table 1. Room temperature properties for a variety of CoorsTek aluminas as reported by CoorsTek [3-4]. CAP3 AD-995 alumina was tested in the present study.

Property	Test	AD-85	AD-94	AD-995	**CAP3 AD-995**
Purity (%)		85	94	99.5	**99.5**
Density (g/cc)	ASTM C20	3.42	3.70	3.90	**3.90**
Average Grain Size (μm)		6	12	6	**6**
Flexure Strength (MPa)	ASTM F417	296	352	379	**379**
Elastic Modulus (GPa)	ASTM C848	221	303	370	**370**
Poisson's Ratio	ASTM C848	0.22	0.21	0.22	**0.22**
Hardness (GPa)	Knoop 1000g	9.4	11.5	14.1	**14.1**
Fracture Toughness (MPa m)	Notched Beam	3-4	4-5	4-5	**4-5**

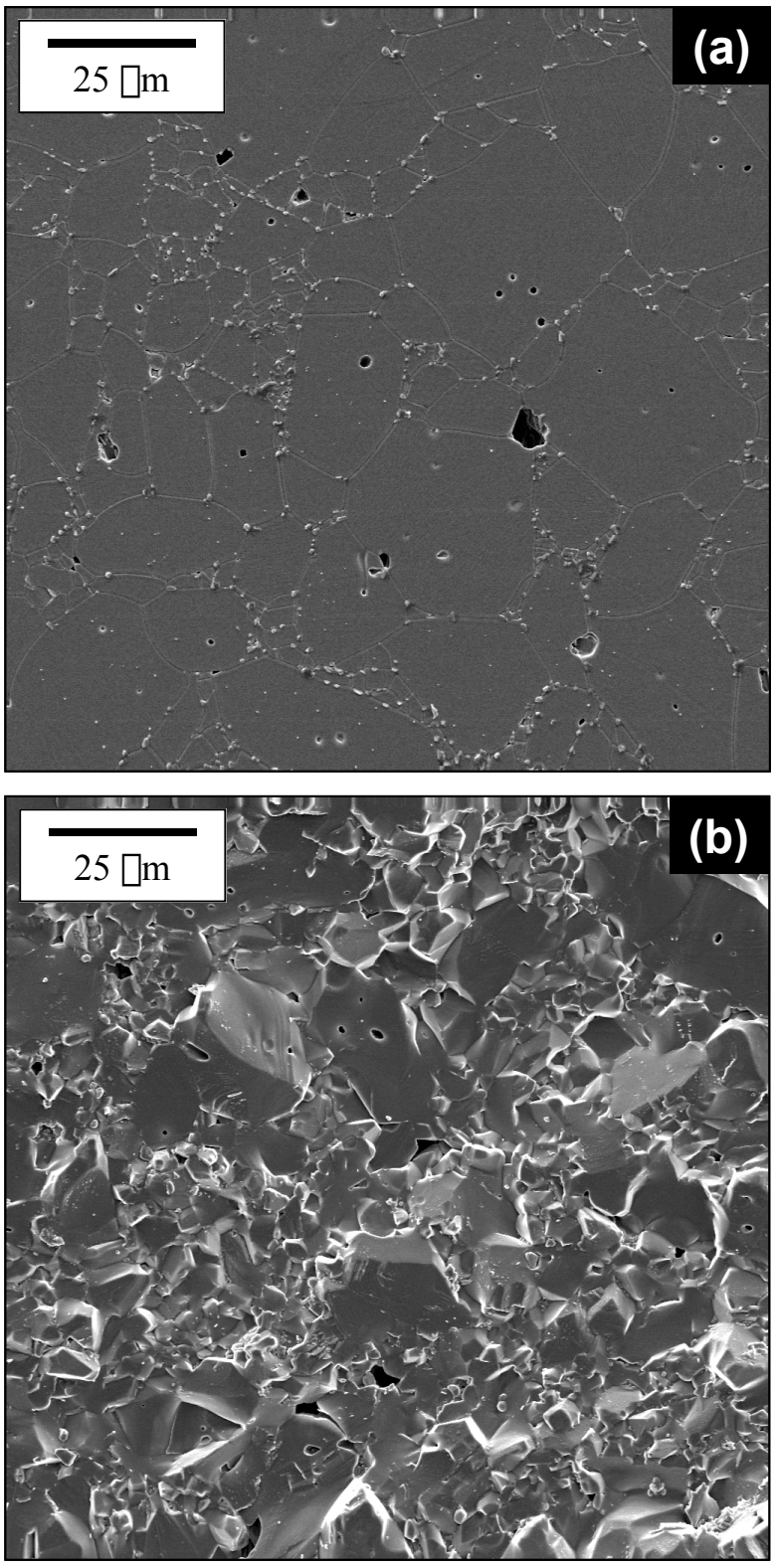

Figure 1. CAP3 AD-995 Al_2O_3 microstructure on a (a) polished and thermally-etched and (b) fractured surface. The latter image shows that transgranular fracture is more dominant than intergranular fracture.

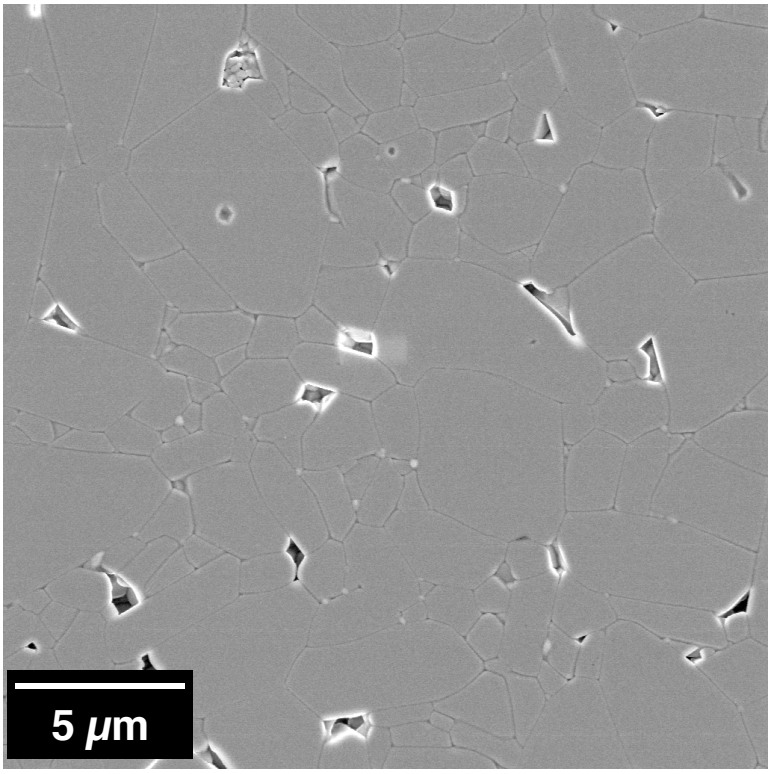

Figure 2. AD-995 Al_2O_3 microstructure - polished and thermally-etched. Though this 99.5%-purity alumina is compositionally equivalent to the CAP3 AD-995 Al_2O_3 tested in this study, its grain size is noticeably smaller (compare to Fig. 1(a)).

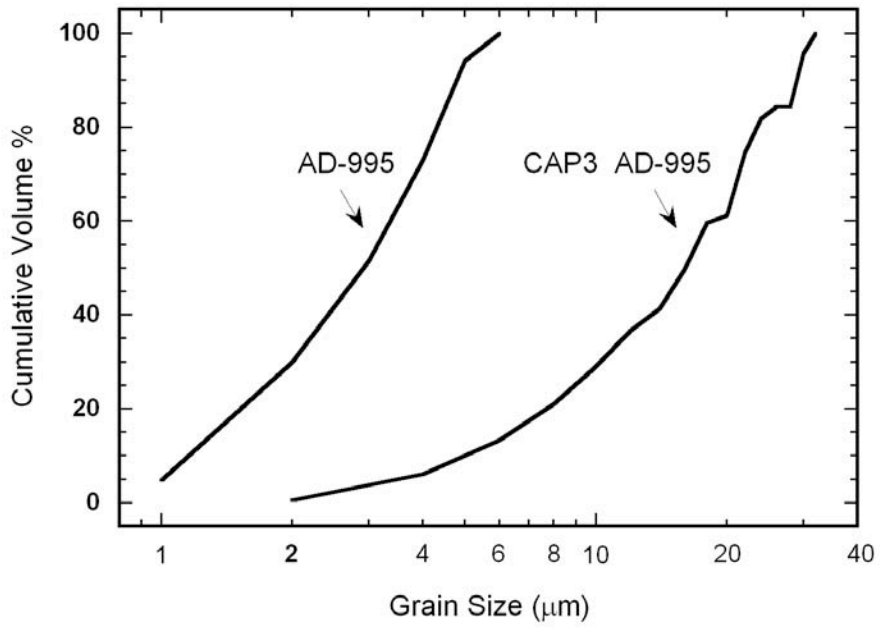

Figure 3. Measured grain size distribution of CAP3 AD-995 (375 grains counted) and AD-995 (166 grains counted).

2.2. Machining Conditions

The surface conditions that comprised the independent parameters of this study are described along with qualitative descriptions of the machining that produced them.

The investigated surface conditions are listed in Table 2. Tiles with nominal dimensions of 4x4x0.118 in. (all ±1%) were purchased from CoorsTek. A fraction of them had "as-fired" surfaces while the remainder had "as-received" ground surfaces that were machined by CoorsTek per their "standard" grinding method. Their "standard" grinding method [7] consists of 80-grit diamond machining and involves rotary surface grinding. This "standard grinding" is the machining practice employed by CoorsTek if a customer of armor tiles only specifies tolerance requirements and not surface finish requirements. It was recognized that many such tiles are purchased having only dimensional tolerance requirements; consequently, it was of interest to characterize strength effect on this "standard" grinding method. The received tile length and width tolerances were within those (± 2.0% or ± 1.5 mm, whichever is greater) specified of per MIL-P-46199 (MR) [2]. Thickness tolerances were within those (± 3.0% or ± 0.5 mm, whichever is greater) allowable MIL-P-46199 (MR) too.

Many of the "as-received" tiles were further machined by a commercial ceramic machining company (Bomas Machine Specialties, Inc., Somerville, MA) with 320-grit diamond machining either using uniaxial or rotary surface grinding. The uniaxial surface grinding procedure (see Fig. 4) is that recommended for machining uniaxial flexure specimens in ASTM C1161-94 [1][1]. Rotary surface grinding (see Fig. 5) using the same 320-grit machining was of interest to see if a non-uniaxial surface grinding procedure yielded equivalent flexure strengths, and because ceramic vendors sometimes prefer to use that method over uniaxial surface grinding.

The final cost per tile for this specific geometry (in 2002 dollars) were as follows: $33/tile for as-fired tiles; $42/tile for "as-received" or CoorsTek machined tiles; and $87/tile for 320-grit uniaxial or rotary surface ground tiles.

Uniaxial flexure specimens were sectioned out of the uniaxial and rotary surface ground tiles in the manner illustrated in Figs. 4-5. Their sectioning out of uniaxial surface ground tiles shows

[1] ASTM C1161B-2002 is now a successor to ASTM C1161B-1994, and it advocates progressive machining steps during grinding with a 400-600 grit wheel used in the final step. The 2002 version was not yet announced at the time the tiles in this study were machined, so the 320-grit finish machining advocated in the 1994 version was employed.

how directionality of machining is oriented with the primary length of the specimen, and portrays the differences in longitudinal and transverse grinding that are listed in Table 2. The tracking and orientation of sectioned uniaxial flexure specimens out of rotary surface grind tiles was not documented. This was unfortunate because the grinding marks on such tiles are a function of the radial tile placement on the work table during machining; however, its effect (if any) on strength was not identified upon examination of equibiaxial flexure strengths.

Table 2. The effects of five surface conditions on strength were investigated. Comparison of cost per tile (nominal dimensions: 4 x 4 x 0.118 in.) shown.

Type of Surface or Descriptor	Description	Cost per tile
As-Fired	Unadulterated surface resulting from sintering of tiles.	$33
As-Received	CoorsTek "standard" grinding method that is used if a customer requests a desired dimension and not a surface finish. It is an 80-diamond-grit rotary grinding process [7]. CoorsTek offers 100-grit grinding for an additional 10% cost, but that was not pursued.	$42
Longitudinal*	Uniaxial surface grinding with a 320-diamond-grit wheel per ASTM C1161-94 [1]. Grinding direction is oriented parallel with the major axis of the bend bar. Such directionality is not exploited by the ring-on-ring equibiaxial flexure testing that was performed in this study.	$87 The 320-grit uniaxial surface grinding ($45) was performed on "as-received" tiles ($42). $87 is their sum.
Transverse*	Uniaxial surface grinding with a 320-diamond-grit wheel per ASTM C1161-94 [1]. Grinding direction is oriented perpendicular with the major axis of the bend bar. Such directionality is not exploited by the ring-on-ring equibiaxial flexure testing.	$87 The 320-grit uniaxial surface grinding ($45) was performed on "as-received" tiles ($42). $87 is their sum.
Rotary Ground*	Rotary surface grinding with a 320-diamond-grit wheel.	$87 The 320-grit rotary surface grinding ($45) was performed on "as-received" tiles ($42). $87 is their sum.

* Bomas Machine Specialties, Inc., Somerville, MA.

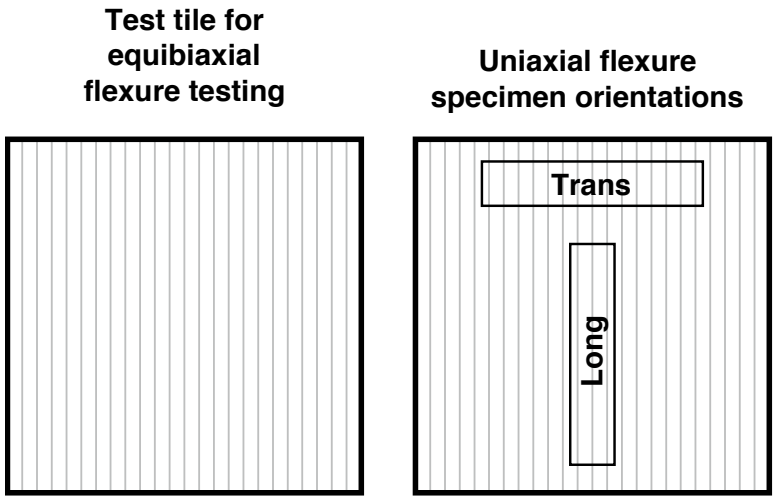

Figure 4. Schematic of grinding mark orientation on uniaxially ground tiles and how transversely and longitudinally machined bend bars were sectioned from them.

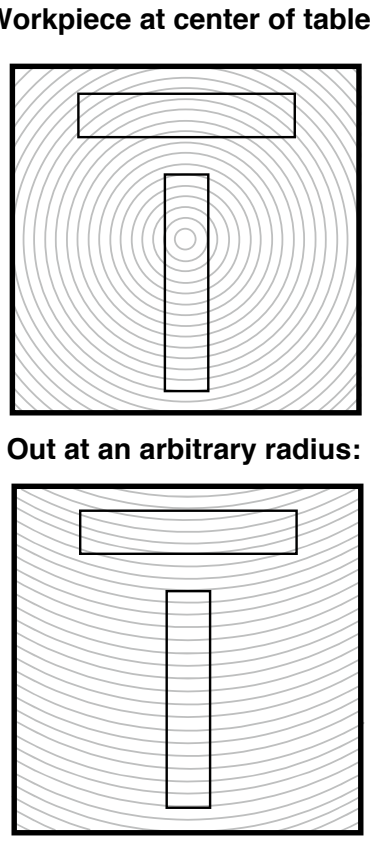

Figure 5. Schematic of grinding mark orientation on rotary ground tiles. Unfortunately, the location (radius) of the tile on the table of the rotary grinder and the orientation of how the how bend bars were machined from the tiles were not monitored.

2.3. Flexure Strength Testing

Uniaxial and equibiaxial flexure strength tests were performed, and established and demonstrated practices were utilized. The surface area sampled by the equibiaxial flexure testing was more than one order of magnitude larger than that sampled by the uniaxial flexure testing, and this exploited the effect of strength-size-scaling in this ceramic.

2.3.1. Uniaxial (ASTM C1161B)

Uniaxial flexure strength testing adhered to ASTM C1161B practices [1] and involved four-point-bending of bars sectioned from tiles that had one of the four surface conditions. One of those conditions, uniaxial surface grinding, was further examined by sectioning specimens both parallel (i.e., longitudinally ground) and perpendicular (i.e., transversely ground) to the direction of uniaxial grinding, so a total of five surface condition sets were examined with uniaxial flexure specimens. A minimum of 27 specimens were tested per surface condition outlined in Table 2. Each of the five surface condition sets were examined by orienting their surface to be on the tensile face of the bend specimen and then tested by uniaxial flexure. A side view schematic of the four-point-bend specimen and fixture is shown in Fig. 6. The specimen dimension was nominally 3 x 4 x 50 mm and it was tested using a fixture having 20 and 40 mm upper and lower spans, respectively. The specimen was monotonically loaded to fracture using a displacement rate of 0.5 mm/min. The failure load (P) was used to calculate the uniaxial flexure strength (S_{1161B}) using

$$S_{1161B} = \frac{3P(L_L - L_U)}{2bh^2} \tag{1}$$

where L_L is the lower span (40 mm), L_U is the upper span (20 mm), b is the specimen base (4 mm) and h is the specimen thickness or height (3 mm).

The effect of chamfered (or unchamferred) bend bar edges on uniaxial flexure strength was also examined. Unchamferred bars from tiles that had as-fired, as-received, and rotary surface ground surfaces were considered. The motivation behind this was to quantify the recognized beneficial effect of edge-chamfering ceramic specimens (and ceramic components too when allowed).

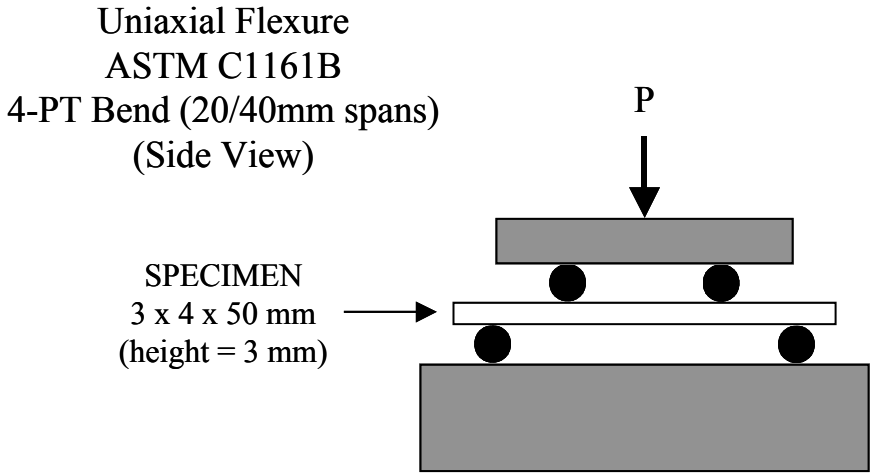

Figure 6. Side view schematic of the uniaxial flexure strength test.

2.3.2. Equibiaxial

Equibiaxial flexure strength testing consisted of concentric ring-on-ring testing of tiles in which the surface condition was oriented to be on the tensile face during equibiaxial flexure.

2.3.2.1. Promoting Valid Equibiaxial Flexure Testing

Much consideration was devoted toward the design of the equibiaxial (concentric ring-on-ring or ROR) flexure fixture, and that was based on prior studies involving this test [8-10]. The ROR configuration is preferred over the piston-on-three ball (PO3B) equibiaxial flexure test (such as ASTM F394 [11]) since it subjects a greater portion of the specimen to an equibiaxial stress state and it distributes the total applied contact load over a larger area of the specimen; this acts to lessen the applied stress concentration at the contact locations between the fixture and specimen which subsequently produces a lesser likelihood of fixture-induced specimen failure (invalid test data). Cimpoeru [12] performed ball-on-elastic foundation study on 99%-purity alumina tiles; though failure load increase was observed with increasing tile thickness as expected, unfortunately no fractography was reported that could have substantiated to the reader that the stress concentration associated with the ball-loading did not cause the fracture events.

Even though the ROR configuration is more advantageous than the PO3B [13], care must still be taken to appropriately determine the diameters of the ROR configuration (relative to the

specimen thickness) in order promote a valid and linear elastic event. For example, if the ratio of the upper ring diameter to the lower ring diameter (D_U/D_L) is too low, then excessive deflection of the specimen can exist at the moment of fracture and result in error being introduced into the calculation of equibiaxial flexure strength due to nonlinear membrane-like stresses and even friction effects. An example of where D_U/D_L is too small and its effect is illustrated in Figs. 7(a) and 8(a); the fixture initiated fracture and therefore a valid equibiaxial flexure strength test was not the result. Conversely, if D_U/D is too high, then contact-stress-concentrations will increase and localized contact-crushing can occur and cause an invalid fracture strength even (and a subsequent invalid equibiaxial flexure strength value). The objective is to determine the range of D_U/D_L where linear elasticity is still valid and contact stresses are minimized; this is accomplished through the appropriate use of classical beam bending (strive to keep maximum deflection below 1/2 of the specimen thickness) and consideration of the materials elastic properties and specimen thickness. When that objective is met, then the test fixture will likely not cause fracture and the intrinsic specimen strength will be measured such as what the fracture patterns in Figs. 7(b) and 8(b) indicate. The ASTM standard, ASTM 1499 [14], for equibiaxial flexure testing follows this rationale.

Fracture patterns in Figs. 7 and 8 are not unlike fracture patterns that are sometimes observed in on-center ballistically evaluated ceramic tiles. Though this commonality is not further explored in this study, it is an important one nonetheless, and provides a glimpse of a possible link between the nature of fracture in equibiaxial flexure testing and that that occurs as a consequence of on-center impact ballistic loading of ceramic tiles.

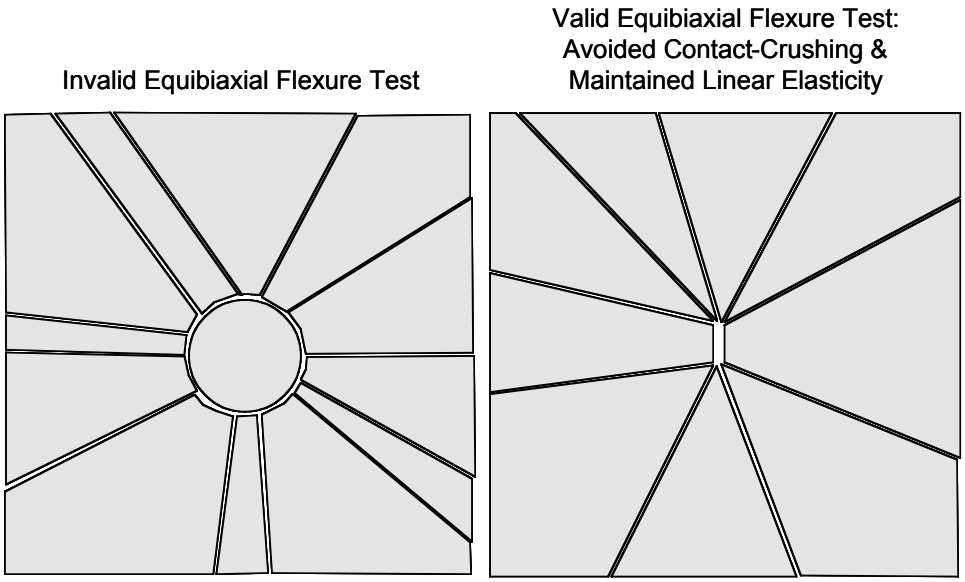

Figure 7. Appropriate determination of the diameters of the ring-pairs with respect to the specimen's elastic properties and thickness will generate a valid equibiaxial flexure strength test. Schematic on the left shows an invalid test (upper ring "punching" a disk through a too-thin specimen). Schematic on the right shows a valid test (the two opposed pieces each having a flat contain the specimen's strength-limiting flaw).

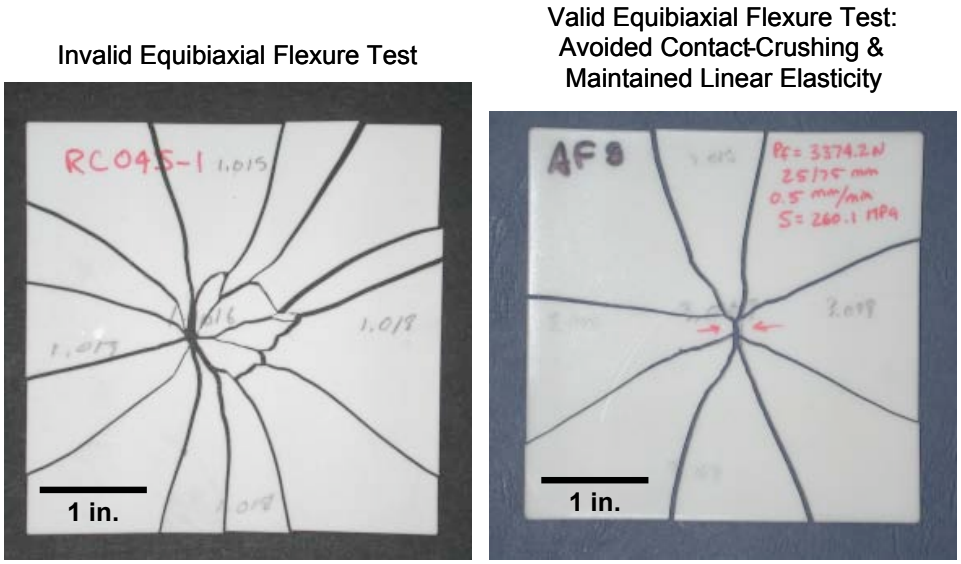

Figure 8. The picture on the left shows an invalid test; the upper ring had "punched" a disk of fragments through the too-thin specimen (i.e., the fixture had caused the fracture event). The picture on the right shows a valid test (i.e., the fixture did not cause the fracture event) and two arrows point to the mating fracture surface where the fracture event was initiated.

2.3.2.2. Description of Fixturing

For the present study, the nominal tile thickness was 3 mm (0.118 in.) and the elastic modulus of the CAP3 AD-995 alumina was approximately 370 GPa. Using principals described in 2.3.2.1 resulted in a choice of a 25 mm diameter for the upper ring and a 75 mm diameter for the lower ring. A schematic of the assembled fixture is shown in Fig. 9 and dimensions, tolerances, and additional detail of the upper and lower rings are included in Figs. 10-11, respectively.

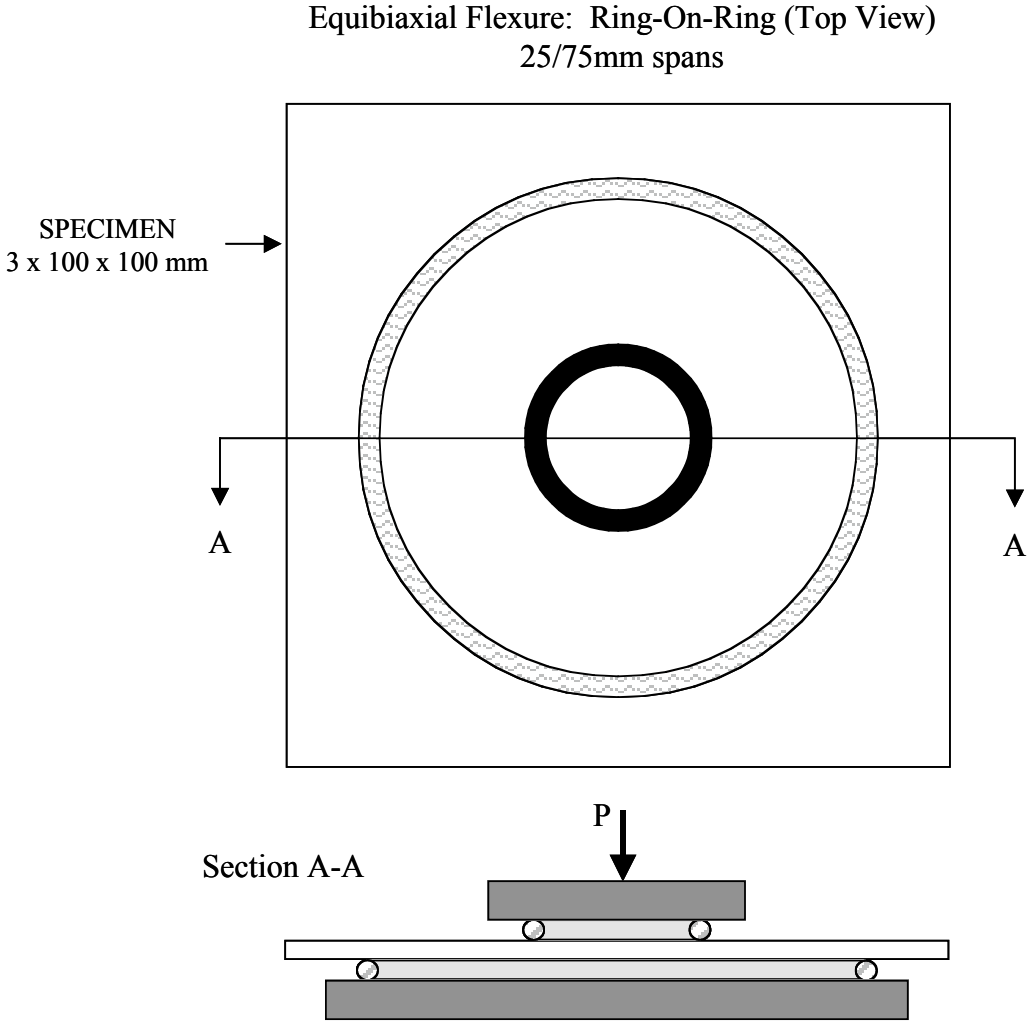

Figure 9. Top and sectioned view schematics of the equibiaxial flexure strength test.

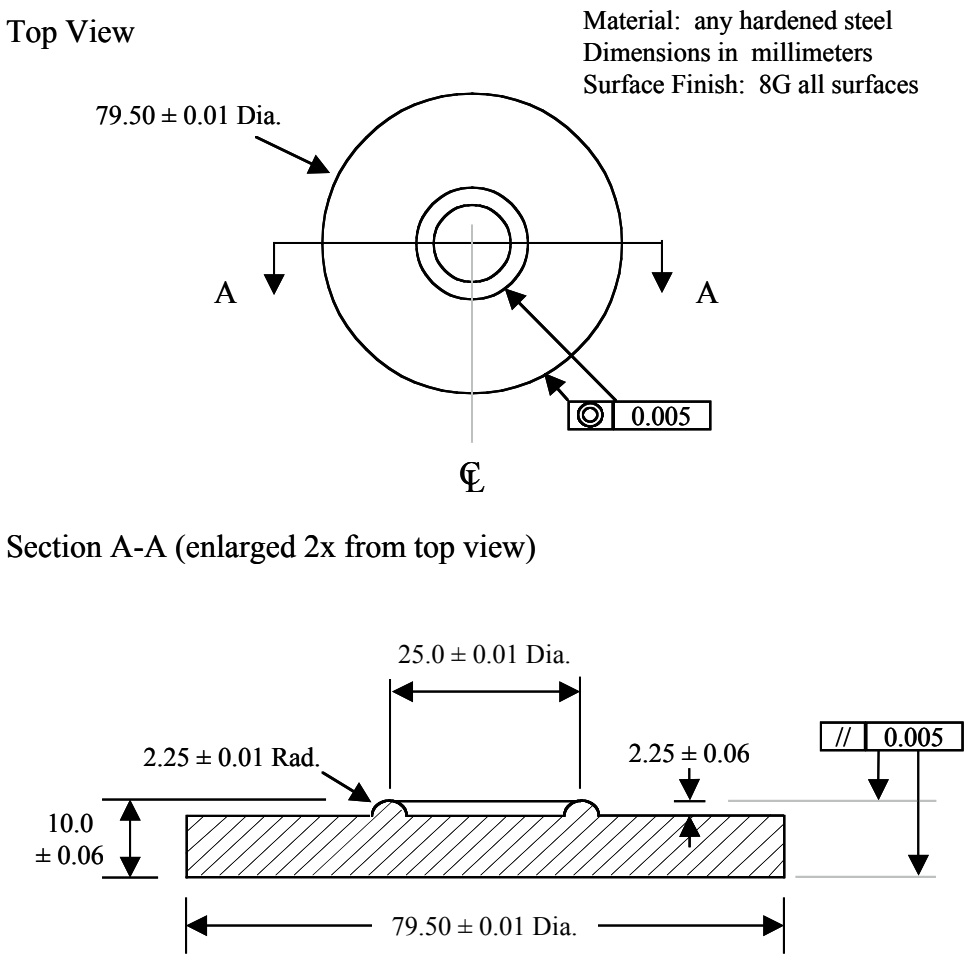

Figure 10. Top and sectioned view schematics of the equibiaxial flexure fixture's upper ring insert (25 mm diameter).

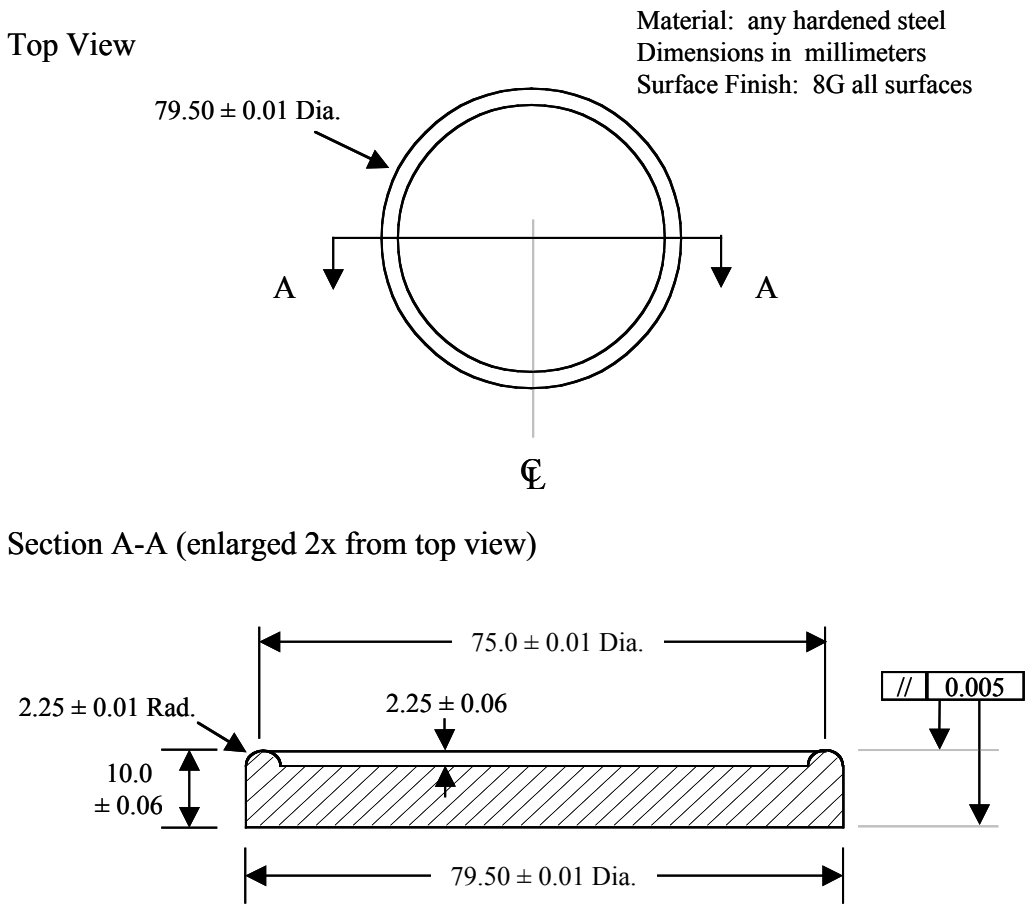

Figure 11. Top and sectioned view schematics of the equibiaxial flexure fixture's lower ring insert (75 mm diameter).

2.3.2.3. Test Procedure

Each tile was inserted in the fixture shown in Fig. 9 and then set in the load train of an eletromechanical universal test machine (Instron Model 1127, Canton, MA). A steel sphere was positioned between the load frame's load cell and the top of the assembled equibiaxial flexure fixture to promote articulated loading (i.e., passive alignment). A displacement rate of 0.5 mm/min was used to load the specimen to fracture.

The equibiaxial flexure strength (S_{ROR}) was calculated using the fracture load (P) and the fixture and tile dimensions according to the following relationship [15-16],

$$S_{ROR} = \frac{3P}{4t^2\pi}\left[2(1+\nu)\ln\frac{D_L}{D_U} + \frac{(1-\nu)(D_L^2 - D_U^2)}{1.2L^2}\right] \quad (2)$$

where t is the tile thickness (~ 3 mm), ν is Poisson's ratio, D_L is the diameter of the supporting or lower ring (75 mm), D_U is the diameter of the loading or upper ring (25 mm), and L is the tile's edge length (~ 100 mm).

A minimum of 6 tiles was tested for each of the four grinding conditions (i.e., as-fired, as-received, uniaxial surface ground, and rotary surface ground). It would have been desirable to have tested a greater number of tiles per condition; however, the statistical analysis took into account these relatively low number of conducted tests in the confidence bound estimations, so strength comparisons having statistically significant resulted still resulted.

2.4. Data and Fracture Analyses

The strength data was analyzed using a two-parameter Weibull distribution, and a description of that application follows. Fractography was performed to identify the type of strength-limiting flaw (as a function of surface condition) in both uniaxial and equibiaxially tested specimens, and a brief description of that effort is presented. Lastly, because the effective areas of the uniaxial and equibiaxial flexure specimens were quite different, a brief description of strength-size-scaling issues in monolithic ceramics is presented.

2.4.1. Two-Parameter Weibull Distribution

The probability of failure (P_f) as a function of failure stress (S) is represented using the uncensored, two-parameter Weibull distribution as follows,

$$P_f = 1 - \exp\left[-\left(\frac{S}{\sigma_\theta}\right)^m\right] \tag{3}$$

where σ_θ is the characteristic strength and m is the Weibull modulus. The adjective "uncensored" in this context means that each measured strength value has not yet been linked to its strength-limiting flaw type. The characteristic strength is a function of the specimen size; however, its value is related to the material scaling parameter which is a material property for a given strength-limiting flaw type. The Weibull modulus is also a material property for a given strength-limiting flaw type. Greater details of the Weibull distribution and its reporting practices for ceramics may be found in ASTM C1239 [17]. The parameters σ_θ and m were determined using the CERAMIC computer program [18] using maximum likelihood estimation (with unbiasing factors) along with 95% confidence bounds about both parameters.

2.4.2. Fractography

The identification of the strength-limiting flaw type was sought in selected uniaxial flexure specimens for each of the five surface conditions (see Table 2). Practices outlined in ASTM 1322 [19] were adhered to. Additionally, the examination of strength-limiting flaw types also occurred with the unchamferred uniaxially flexure specimens. Lastly, selected equibiaxial flexure specimens from each of the four unique surfaces (i.e., as-fired, as-received, uniaxial surface ground, and rotary surface ground) were examined. The fractography was performed using reflected light optical microscopy (RLOM) or secondary electron imaging with scanning electron microscopy (SE-SEM) or both.

2.4.3. Strength-Size-Scaling

Strength-size-scaling with surface area (when strength-limiting flaws are restricted to the specimen surface) or volume (when strength-limiting flaws are volumetric in nature) has long been recognized as a characteristic associated with monolithic ceramics. The following description pertains to strength-size-scaling analysis associated with surface area; analogous analysis associated with volume is not presented.

When surface flaws are strength-limiting, the Weibull distribution for strength-size-scaling is represented by

$$P_f = 1 - \exp\left[-k_A A \left(\frac{S}{S_{OA}}\right)^m\right], \quad (4)$$

where k_A is the area loading factor, A is area of the specimen subjected to tensile stress, and S_{OA} is the material's area scaling parameter (and has units of $MPa\cdot(mm^2)^{1/m}$). The product of $k_A A$ is typically referred to as the effective area. The loading factor (also called the stress gradient factor) represents the failure stress dependence on the specimen configuration and the (tension) loading conditions. The loading factor has a range of $0 < k_A \leq 1$; it is equal to one only for pure uniaxial tension; and is a function of the Weibull modulus when $k_A < 1$. The loading factor's dependence on m is analytic for simple test geometries and loadings, but its calculation and dependence on m requires numeric determination for complex shapes, loadings, or service boundary conditions. The trend of Eq. 4 shows that higher probabilities of failure exist when greater surface area of a ceramic is subjected to the same tensile stress.

The effective area for ASTM C1161B, $(k_A A)_{1161B}$, is [20],

$$(k_A A)_{1161B} = \frac{m+2}{2(m+1)}\left[bL_L + \frac{hL_L}{m+1}\right] \quad (\text{units} = mm^2), \quad (5)$$

where b is the specimen width (4 mm), h is the thickness or height (3 mm), and L_L is the lower loading span (40 mm). The effective area for ASTM C1161B is illustrated in Fig. 12 as a function of Weibull modulus (m).

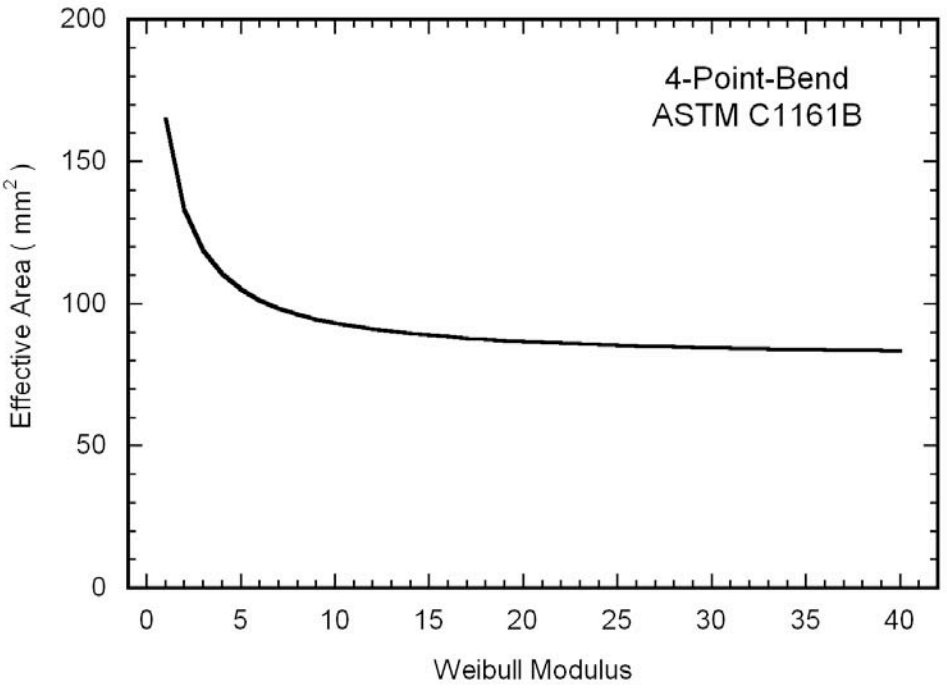

Figure 12. The effective area for the ASTM C1161B uniaxial flexure specimen as a function of Weibull modulus.

A multiaxial stress state obviously exists in equibiaxial flexure testing, and the calculation of the effective area is more complex since an assumption regarding the effect of a multiaxial fracture criterion must be considered. Batdorf [21] and Breder [22] considered this, and combining that analysis with the fixture geometry used in the present study, results in the following relationship for the effective area for a ring-on-ring, $(k_A A)_{ROR}$, equibiaxially tested specimen

$$(k_A A)_{ROR} = 2\pi r_U^2 m^{0.45} = 981.7 m^{0.45} \quad (\text{units} = \text{mm}^2), \tag{6}$$

where r_U is the radius of the upper loading ring (25 mm in this study). The effective area for this study's equibiaxial flexure testing as a function of Weibull modulus is illustrated in Fig.13.

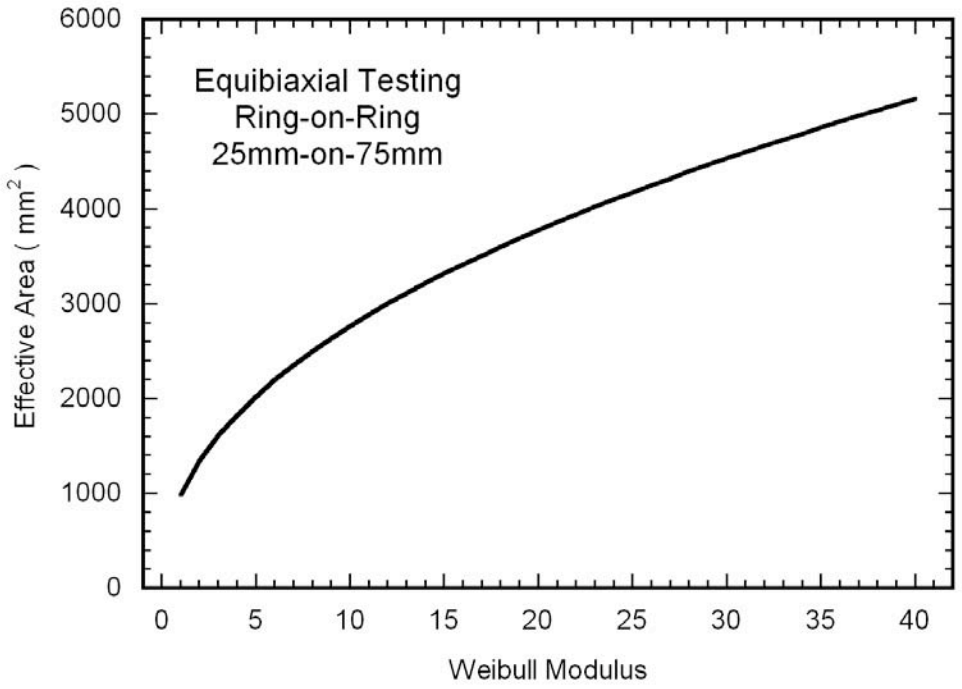

Figure 13. The effective area for the utilized equibiaxial flexure test as a function of Weibull modulus according to Eq. 6. This expression is only representative for the equibiaxial fixture geometry used in the present study (i.e., upper ring diameter of 25 mm) and Batdorf's multiaxial fracture criterion [21].

For the same strength-limiting surface flaw, the failure stresses of the two specimen geometries may be related according to

$$\frac{S_{1161B}}{S_{ROR}} = \left[\frac{(k_A A)_{ROR}}{(k_A A)_{1161B}}\right]^{1/m} . \qquad (7)$$

The percentage of the failure stress for the equibiaxial flexure strength to that of the uniaxial flexure strength is illustrated in Fig. 14 as a function of Weibull modulus. For example, for a ceramic that has a Weibull modulus of 20, the equibiaxial failure stress (for the test geometry used in the present study) will be approximately 80-83% of the uniaxial failure stress for any given failure probability.

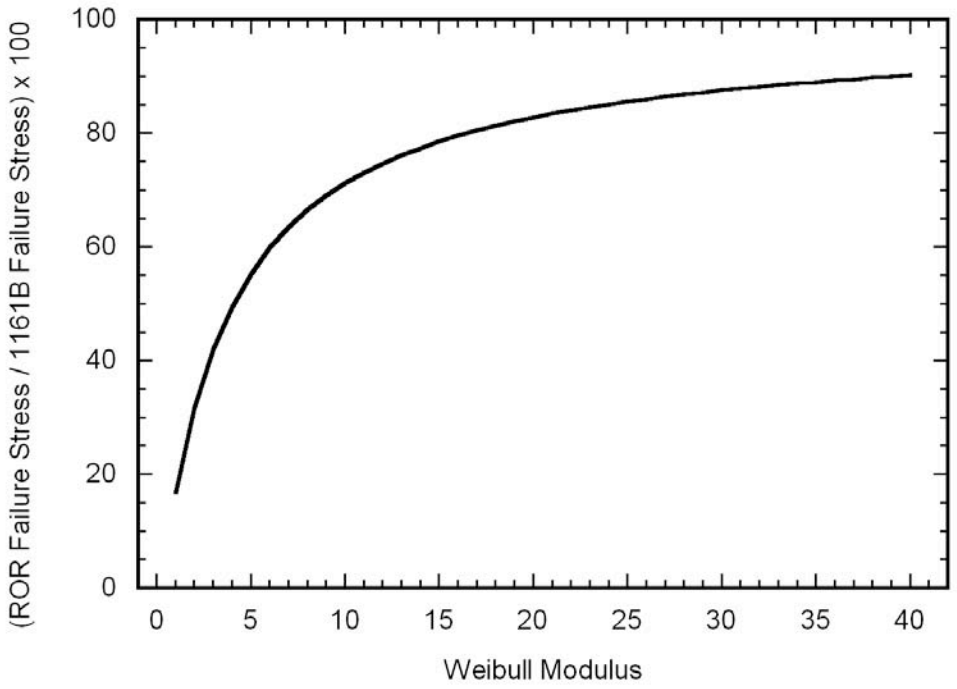

Figure 14. Percentage of the failure stress for the present study's equibiaxial flexure to that of the uniaxial flexure failure stress.

CoorsTek reports (see Table 1) an ASTM F417 [23] uniaxial flexure strength of 379 MPa for CAP3 AD-995 alumina; however, this strength value, if not strength-size-scaled to the more commonly referred to ASTM C1161B geometry, appears relatively high and can be misleading. For example, if the F417 strength of CAP3 AD-995 alumina was limited by surface flaws and had a Weibull modulus of 20, then its effective area would only be 2.28 mm^2, and its scaling to ASTM C1161B using Eq. 7 show that its expected strength would be only 316 MPa (a 20% decrease).

An issue worthy of greater discussion is that the proper utilization of Equations 4-7 is predicated on the fact that *surface-type* flaws are the strength limiter. This may appear to be a moot point; however, the symantics of flaw-type v. flaw-location can cause confusion if their differences are not understood. For example, a volume-type flaw (e.g., an abnormally large grain) located in the interior of a specimen or component is a volume-type volume-located flaw, and a volume-type flaw that happens to be located at the surface is not a surface-type flaw, rather, it is a surface-located volume-type flaw, etc. When volume-type flaws (a 3-dimensional entity) are located at a surface (a 2-D domain) or at an edge (a 1-D domain), analogous equations

for volumes that are analogous to Eqs. 4-7 for surfaces must be utilized. Similarly, when a surface-type flaw (a 2-D entity that obviously cannot be located within the volume) is located at an edge , then Eqs. 4-7 would be used. Edge-type flaws are unique in that they (obviously) can only be located at edges, and analogous equations to Eqs. 4-7 for edges would be used for component design when the component has edges. A temptation of data censoring is to solely identify flaw location over flaw type (the latter is much more laborious to identify); though the identification of location is useful to know, its information is insufficient as input for established probabilitistic design and life analysis. Strict data censoring was outside the scope of the present study, so the strength-size-scaling analysis conducted (i.e., Eqs. 4-7) among the two test geometries assumed that surface-type flaws (i.e., those generated from machining) were the strength-limiters.

3. Results and Discussion

3.1. Strength as a Function of Surface Condition

Strength depended on surface condition both for uniaxially (Fig. 15) and equibiaxially (Fig. 16) tested specimens, and is summarized in Table 3. Surfaces that were uniaxial or rotary ground using 320-grit diamond machining generated the highest strengths (equibiaxial flexure characteristic strength = 280 MPa) CAP3 AD-995 alumina, followed in descending order of strengths from as-fired surfaces (equibiaxial flexure characteristic strength = 264 MPa), and then strengths from surfaces produced by CoorsTek's standard grinding procedure (equibiaxial flexure characteristic strength = 244 MPa). Those differences in strengths are statistically significant with 95% confidence. These results show 320-grit machining can increase flexure strength, and suggest that CoorsTek's standard surface grinding procedure of CAP3 AD-995 tiles is perhaps too aggressive if strength-retention is required.

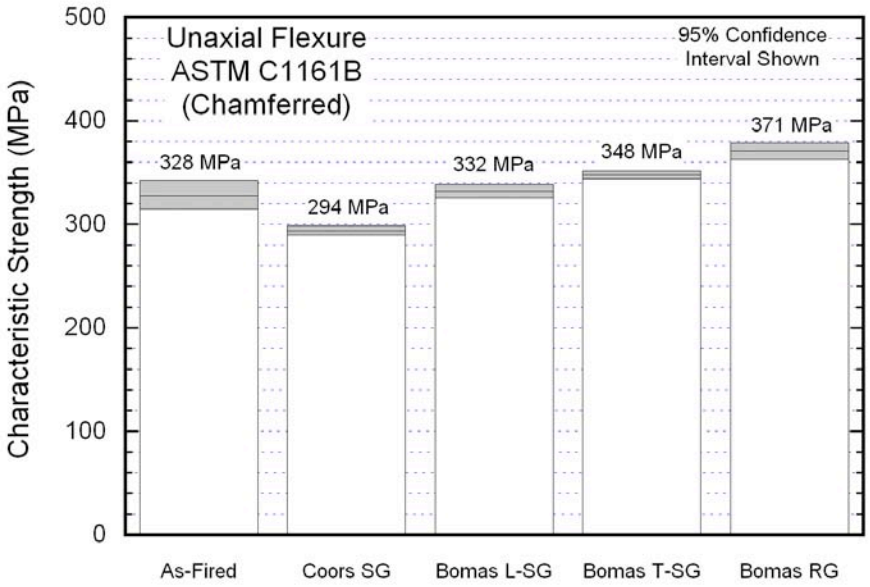

Figure 15. Comparison of characteristic strengths for uniaxial flexure tests of specimens with chamfered edges. SG = surface ground; RG = rotary ground; L = longitudinally ground; and T = transversely ground.

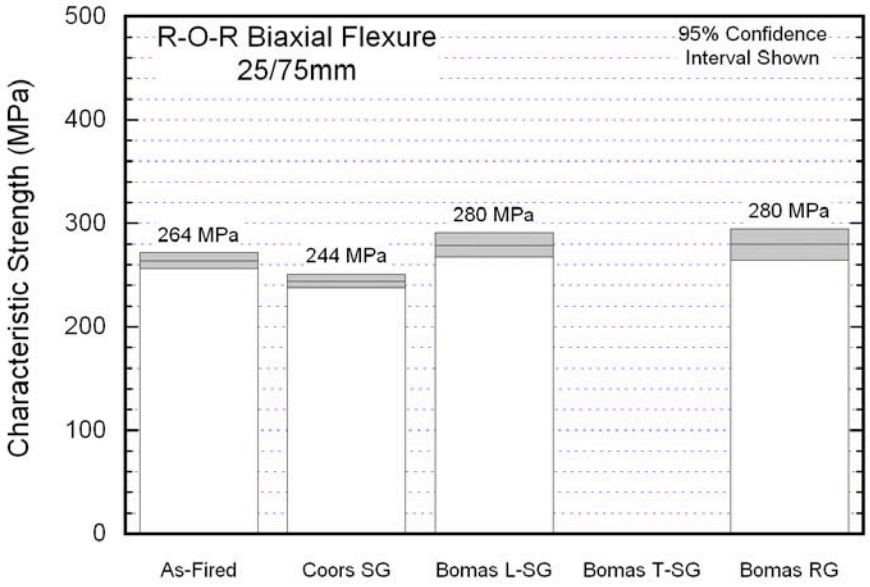

Figure 16. Comparison of characteristic strengths for equibiaxial flexure. SG = surface ground; RG = rotary ground; L = longitudinally ground; and T = transversely ground. Bomas L-SG and Bomas T-SG are equivalent for equibiaxial flexure testing.

Table 3. Two-parameter Weibull strength distributions and their 95% confidence estimates.

Surface Condition	Test Type	# of tests	RH (%)	Uncensored Characteristic Strength, σ_0 [± 95% Conf. Est.] (MPa)	Uncensored Weibull Modulus, m [± 95% Conf. Est.]
As-Fired	Uniaxial - chamfer	30	55	328 [315, 343]	8.8 [6.3, 11.9]
	Uniaxial - no chamfer	30	44	310 [301, 319]	13.3 [9.8, 17.3]
	Equibiaxial	13		264 [256, 272]	19.6 [12.1, 29.0]
As-Received	Uniaxial - chamfer	30	55	294 [290, 299]	23.7 [17.1, 31.4]
Rotary Ground	Uniaxial - no chamfer	30	62	283 [279, 287]	26.5 [19.6, 34.5]
(80-grit)	Equibiaxial	6		244 [238, 251]	39.9 [18.9, 69.5]
Longitudinal	Uniaxial - chamfer	28	55	332 [326, 339]	20.4 [14.8, 27.0]
	Equibiaxial *	6		280 [268, 291]	25.4 [11.9, 45.2]
Transverse	Uniaxial - chamfer	28	35	348 [344, 352]	33.6 [24.7, 43.6]
	Equibiaxial *	6		280 [268, 291]	25.4 [11.9, 45.2]
Rotary	Uniaxial - chamfer	27	34	371 [363, 379]	18.4 [13.1, 24.8]
Ground	Uniaxial - no chamfer	27	62	343 [337, 349]	24.1 17.3, 32.0]
(320-grit)	Equibiaxial	6		280 [265, 295]	19.6 [9.2, 35.0]

* Same data.

Note: RH was inadvertently not measured when the equibiaxial flexure tests were conducted; however, they were all tested on the same day (and believed to have been subjected to the same RH).

The extra cost of machining CAP3 AD-995 alumina, and their effects on strength, are somewhat enigmatic. First, though CoorsTek's "standard" machining will of course provide a tile whose dimensions will have stricter tolerances than those of "as-fired" tiles for an extra cost of $14/tile, that comes at the expense of lower flexure strengths - a 7-8% decrease. The strength of 320-grit machined tiles was 6% and 15% greater than tiles with as-fired surfaces and CoorsTek "standard" ground surfaces, respectively, but that resulted from an additional expense of $45/tile. If desire remains to have CoorsTek perform the surface machining of their CAP3-AD995 alumina tiles and strength-reduction is not allowable, then a requested combination of a less aggressive machining practice and a finer grit grinding wheel should be made by the customer. Clearly, the 320-grit machining benefits strength; however, the justification of the extra expense for that relatively low amount of strengthening is subjective.

As expected, chamfered edges on specimens had a beneficial effect on uniaxial flexure strength. *Not* chamfering uniaxial flexure specimens resulted in a strength loss of approximately 4-8% for a given machining condition for CAP3 AD-995 alumina, see Figs. 17-21 and Table 3. The reduction in strength correlated with failure consistently being initiated at the edge of these specimens (an occurrence not observed when bend bar edges were chamfered). A lack of edge chamfering inherently has no effect on equibiaxial flexure strength; however, it indeed may as a tile is mechanically loaded closer to one of its edges (and that edge is chamfered or unchamferred). Chamfering edges in ceramic specimens and components has been long recognized to increase strength; however, in spite of that recognized effect, the study of chamfered or unchamferred edges in the present study was revisited because ceramic tiles still in fact are purchased with unchamferred edges and interest therefore existed to statistically illustrate their detrimental effect on strength.

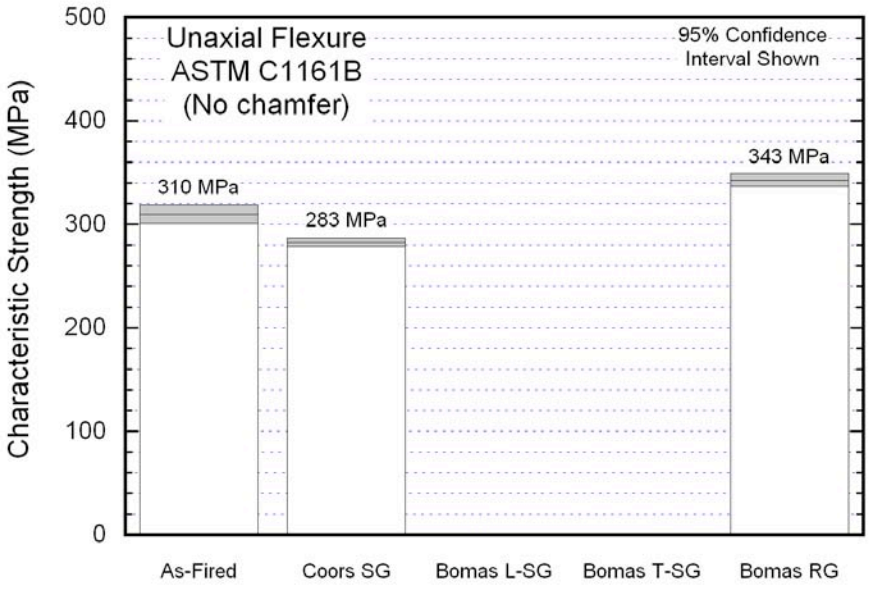

Figure 17. Comparison of characteristic strengths for uniaxial flexure tests of specimens without chamfered edges. SG = surface ground; RG = rotary ground; L = longitudinally ground; and T = transversely ground.

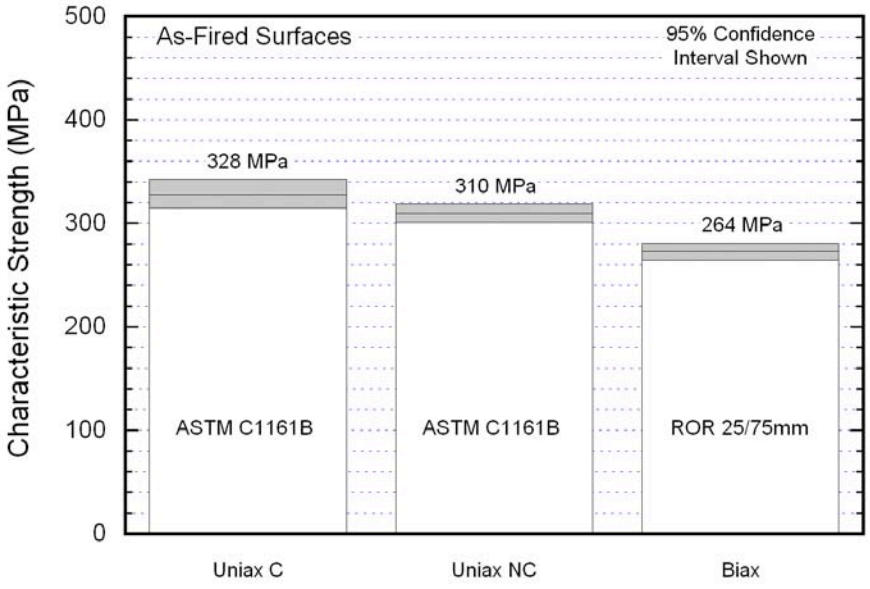

Figure 18. Comparison of characteristic strengths for the three different test types for specimens with as-fired surfaces.

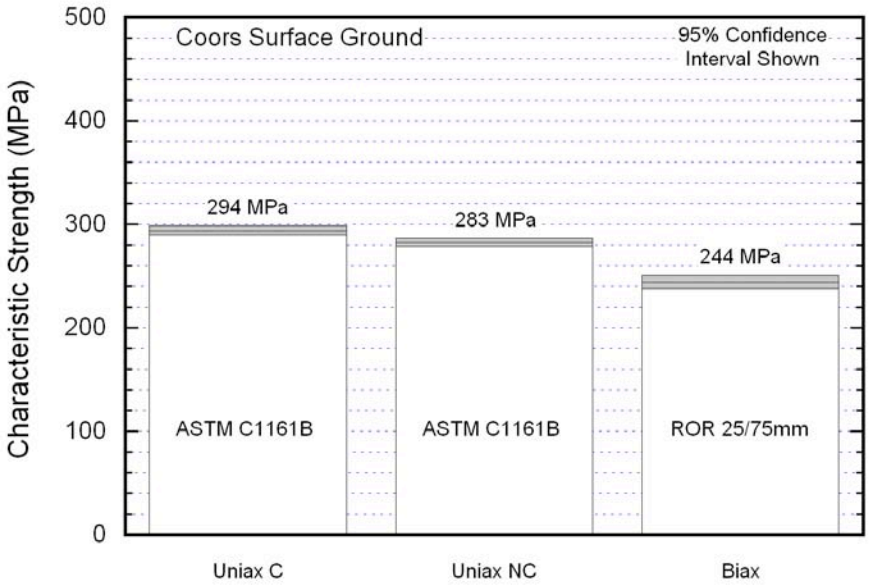

Figure 19. Comparison of characteristic strengths for the three different test types for specimens with as-received (80-grit surface ground) surfaces.

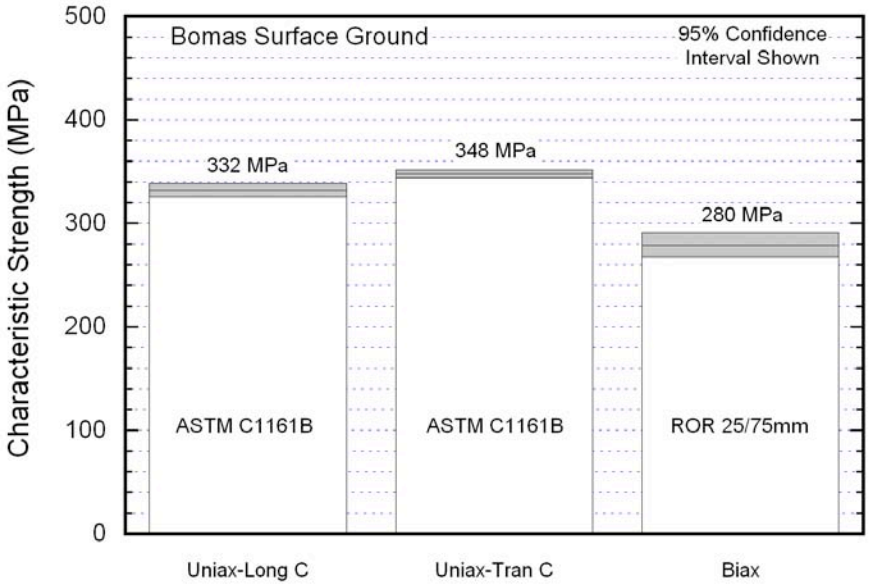

Figure 20. Comparison of characteristic strengths for longitudinally- and transversely-machined (chamfered) ASTM C1161B bend bars and equibiaxial tested tiles with 320-grit surface ground surfaces. The effect of chamfering was not explored with this surface condition.

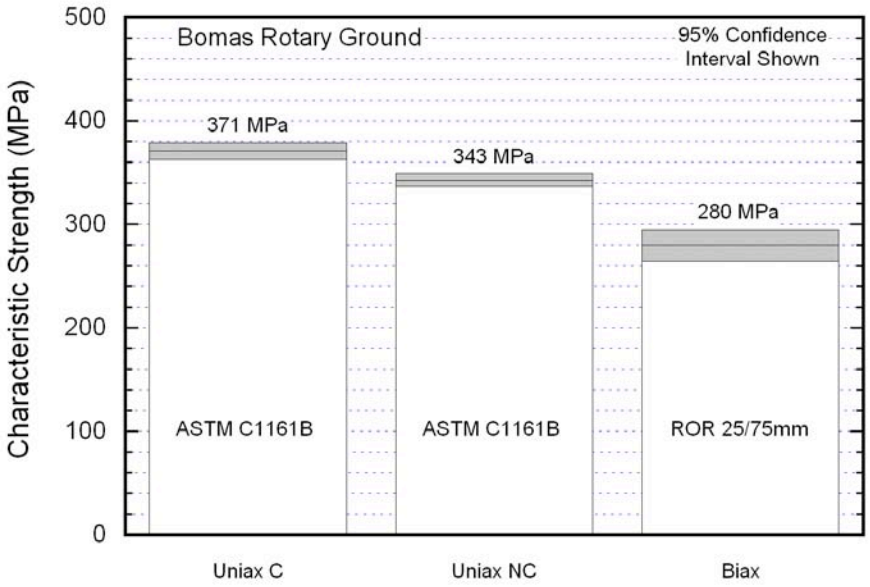

Figure 21. Comparison of characteristic strengths for the three different test types for specimens with rotary ground (320-grit machined) surfaces.

Uniaxial flexure testing with ASTM C1161B-94 produced strengths that were dependent upon machining direction, whereas equibiaxial flexure strengths inherently did not because of the nature of its associated stress state. The directional-dependence on uniaxial flexure strength was a consequence of the interaction between the extent of anistropic machining damage and the relatively large average grain size of CAP3 AD-995 alumina. Though directional dependence on uniaxial flexure strength was anticipated, it was expected that the uniaxial flexure strength of the longitudinally-machined ASTM C1161B would be larger than that for transversely-machined bars as the literature is densely populated with such observations for fine-grained polycrystalline ceramics [24-27]; however, the opposite trend was observed with this coarse-grained CAP AD-995 alumina. The directional-dependence on uniaxial flexure strength effect only complicates the general interpretation of flexure strength's dependence on surface condition, whereas equibiaxial flexure testing facilitates surface condition comparisons because of its "averaging effect" on machining directionality - it is perhaps a better flexure test for assessing flexure strength of armor tiles.

Rice [28-29] found for a variety of ceramics that the ratio of transversely-ground strengths to longitudinally-ground strengths exhibited a maximum when those ceramics had a relatively large average grain size. For example, the ratio of those two strengths was reported to be approximately unity when alumina had an average grain size of approximately 20 μm, and that ratio decreased when the average grain size was both finer and coarser than that size. Rice attributed this maximum ratio of 1 to be a consequence of the strength-limiting flaw size (more specifically, the flaw shape) to be constrained by the (relatively large) grain size. Machining-induced flaws tend to be elongated (i.e., semi-elliptical) for finer grained ceramics whose average grain sizes are smaller than the size of the strength-limiting flaw; however, larger grained ceramics affect/interact with the shape of that machining-induced flaw with the ultimate effect that there is a specific grain size of a ceramic where the strength is independent of the direction of machining. The CAP3 AD995 results in the present study are consistent with those results in that the strengths measured with the transversely-ground bend bars were equivalent (or even slightly higher) than the strength measured with the longitudinally-ground bend bars.

Residual stresses due to machining were considered as a possible contributor to the result that the characteristic strength of transversely-machined bend bars was higher than that of longitudinally-machined bend bars but were found to play an insignificant role. Machining produces a compressive residual stress field on surfaces with greater compressive stresses perpendicular to the grinding direction than parallel with it [30]. Piezoluminescence measurements on the ground surfaces of selected specimens from all five test specimen sets were performed, and even though they sample a hydrostatic stress, their results showed that the residual compressive stresses were relatively small in magnitude (see Table 4) for all the different investigated ground (and unground) surfaces and could not be used to reconcile the different characteristic strengths among those sets. For example, if one set had a characteristic flexure strength of 400 MPa and there were no residual compressive stresses on the tensile surfaces of those specimens, and second set had a characteristic flexure strength of 500 MPa yet contained a residual compressive stress of 100MPa (all other things being equal), then the presence of the residual compressive stress on the latter set causes that set to have a higher flexure strength. The characteristic strength differences among investigated sets were on the order of many tens of MPa, whereas the differences in the compressive residual stresses among

those sets were much smaller than that, and therefore cannot be used as an explanation for those differences in characteristic strengths.

Table 4. Surface Residual Stress Measured via Piezoluminescence.

Surface Condition	Specimen	Fracture Strength (MPa)	Hydrostatic Stress (MPa)	Hydrostatic Stress Std dev. (MPa)
As-Fired	AF2	334.0	-5	6
	AF3	289.3	-11	17
	AF4	357.9	1	15
As-Received	AR1	296.0	-12	32
Rotary Ground	AR2	303.9	-36	19
(80-grit)	AR3	302.0	-24	23
Longitudinal	L1	327.4	-24	10
	L2	325.7	-23	11
	L3	341.3	-21	11
Transverse	T1	352.1	-5	25
	T2	348.5	-26	25
	T4	344.2	-11	14
Rotary	R2	346.0	-33	31
Ground	R3	360.4	-16	11
(320-grit)	R4	321.8	-25	17

Tensile surface of bend bars evaluated. Spot size ~ 2 μm, and penetration depth ~ 5 μm.

There is evidence to suggest that higher relative humidities (RH) can result in lower strengths (about a 10% strength decrease between 30 and 60% RH) in fine-grained AD995 alumina [31-32]; however, none of the five sets were tested under conditions of differing RH (i.e., each set was tested in one-day when RH was presumably unchanged during the testing) so it cannot be concluded that RH affected any of the strengths measured in the present study. Additionally, though the purities of the alumina in that previous work showing strength dependence on RH and the alumina studied in the present study were the same, it is not known if the microstructures were equivalent as their authors did not report such information. This information is an unfortunate omission as average grain size in such commercially available aluminas can vary by almost an order of magnitude. The characteristic strength of the transversely-machined set in the present study was approximately 5% greater than that of the longitudinally-machined set, and the RH was higher on the day that the latter was tested, so the trends in strength and RH between them are consistent with findings from the work of Cho, et al. [31-32]; however, the above-described and more completely-documented effect of grain size on strength-anisotropy is believed to be the primary cause of the strength differences in the transversely- and longitudinally-machined sets.

3.2. Strength-Limiting Flaws

The measure of the flaw origin size, a, (i.e., depth of a surface flaw) can be estimated using the Griffith Equation,

$$a = \left(\frac{K_{Ic}}{Y \sqrt{\sigma}} \right)^2 , \qquad (8)$$

where K_{Ic} is the fracture toughness, σ is the fracture surface at the origin, and Y is a stress intensity shape factor for the origin. If a fracture toughness of 4 MPa $\sqrt{m}$ is considered in Eq. 8 along with the extreme values of Y associated with circular or semielliptical flaw shapes [19], then the strength-limiting surface flaw size for the characteristic strengths listed in Table 3 should range in size between approximately 30 and 160 μm. Examples of strength-limiting flaws are shown in Figs. 22-27 for the five respective surface conditions listed in Table 2 and for an unchamferred bend bar. The flaws were almost always volume-type flaws

(e.g., agglomerates, regions of large grains) that were located on, or near, the surface and that even appeared to be hybridized with machining damage in those sets that involved machining (i.e., not the as-fired surface condition). Edge failures existed in many of the unchamferred bend bars.

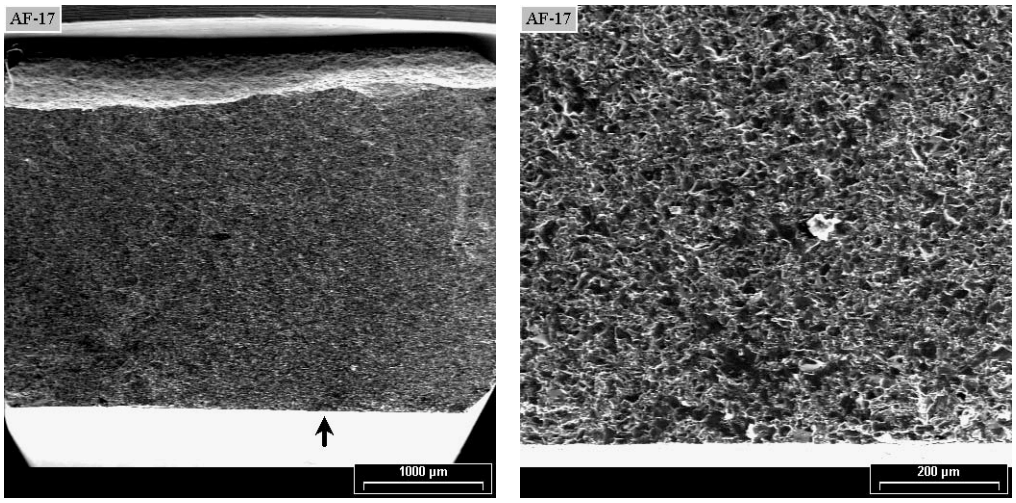

Figure 22. Fracture surface of an As-Fired, chamfered, ASTM C1161B bend showing (left) failure location and (right) higher magnification image of the location containing the strength-limiting flaw.

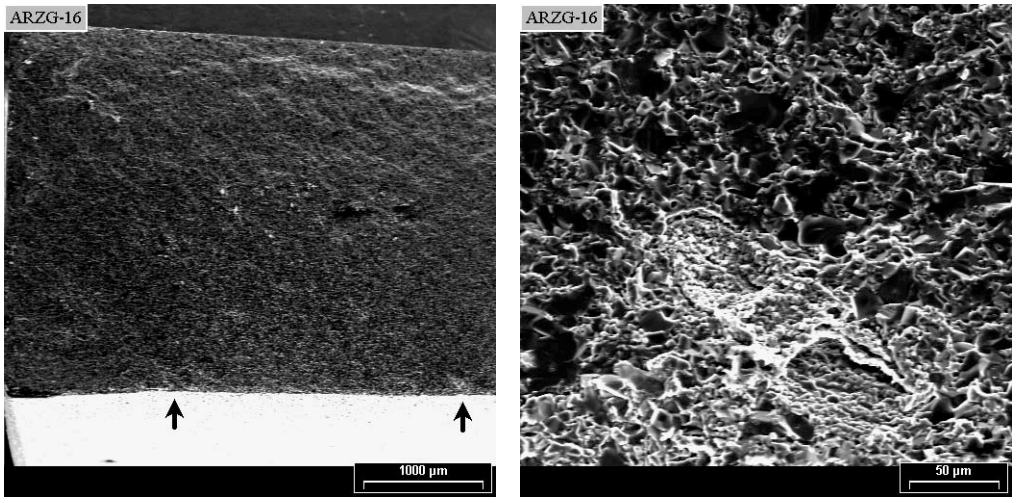

Figure 23. Fracture surface of an As-Received, CoorsTek ground, chamfered, ASTM C1161B bend showing (left) failure location and (right) higher magnification image of the location containing the strength-limiting flaw.

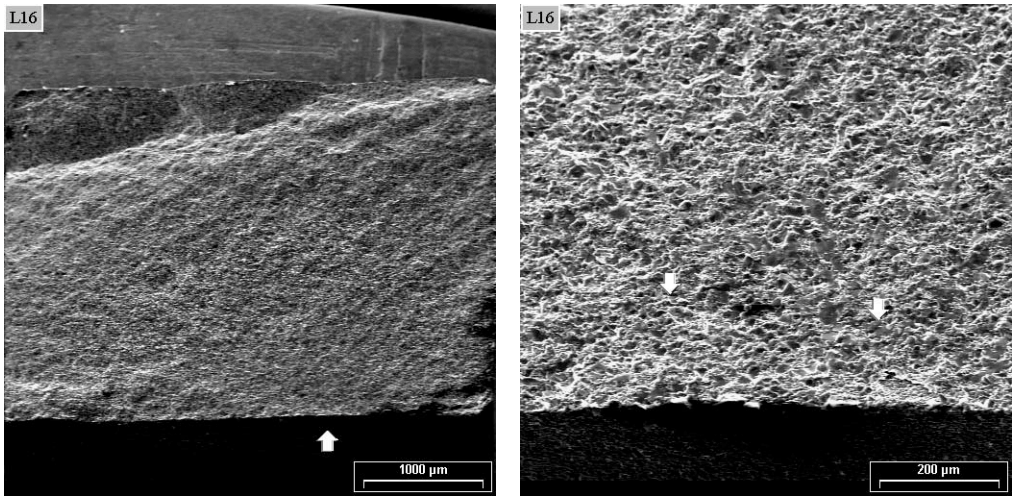

Figure 24. Fracture surface of a longitudinally-ground, chamfered, ASTM C1161B bend showing (left) failure location and (right) higher magnification image of the location containing the strength-limiting flaw.

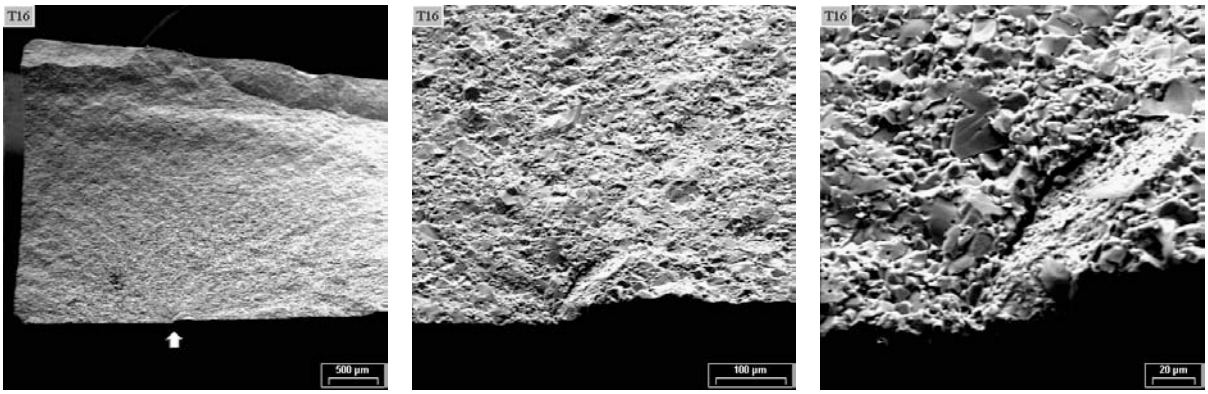

Figure 25. Fracture surface of a transversely-ground, chamfered, ASTM C1161B bend showing (left to right) progressively higher magnification images of the location containing the strength-limiting flaw.

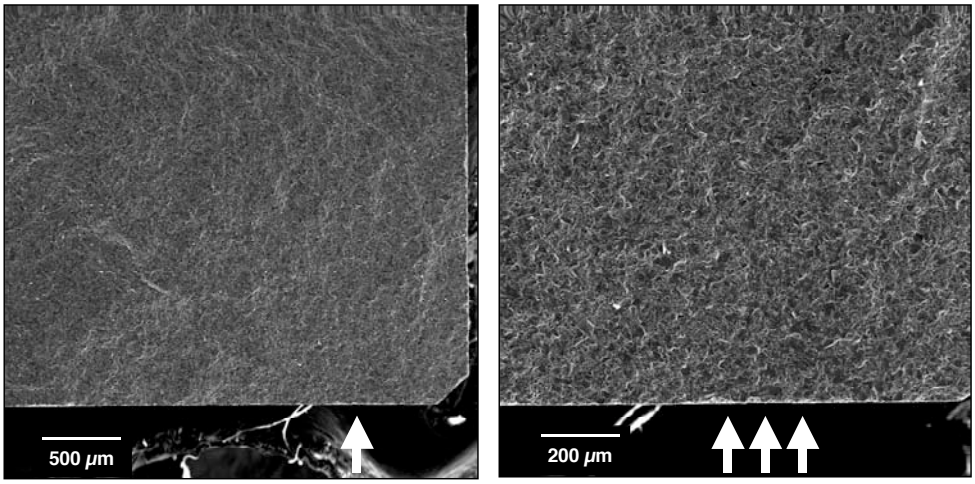

Figure 26. Fracture surface of a rotary-ground, chamfered, ASTM C1161B bend showing (left) failure location and (right) higher magnification image of the location containing the strength-limiting flaw.

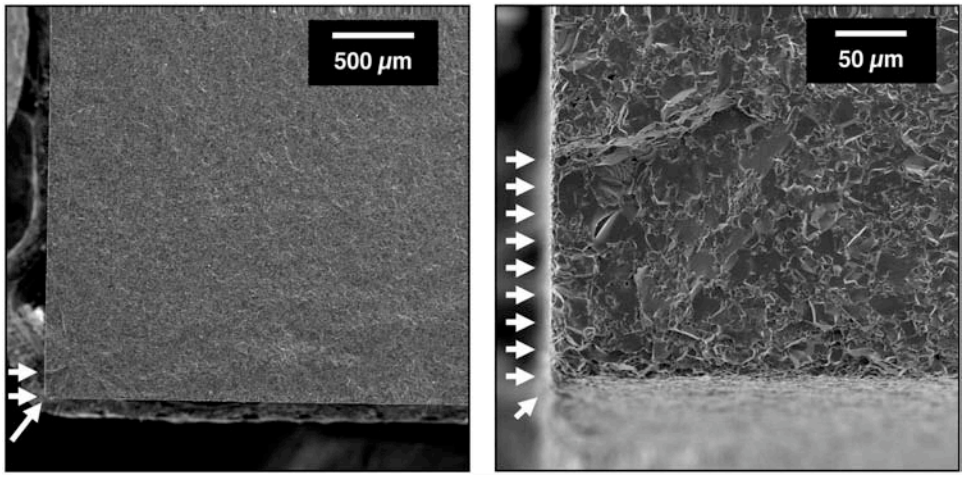

Figure 27. Fracture surface of an As-Received, CoorsTek ground, unchamfered, ASTM C1161B bend showing (left) failure at the corner and (right) higher magnification image of the location containing the strength-limiting flaw.

3.3. Strength-Size-Scaling

Equibiaxial flexure strengths were ~ 20% less than uniaxial flexure strengths for any of the four investigated surface conditions: this amount correlates very well with predicted strength-size-scaling between the two geometries using Weibull theory and Eq. 7. Because this failure stress is lower, and probably more representative of on-center ballistic loading of ceramic tiles, its use is desirably conservative and perhaps better suited as input in ballistic models that consider such deflections.

3.4. Closing Comments

The results from this study show that machining practices can be employed to increase flexure strength that can potentially have beneficial ramifications on ballistic performance when tile thickness is influential (i.e., relatively thin). An illustration of this argument is shown in Fig. 28, and its content is consistent with other reports describing the nature and chronologies of impact-induced crack and fracture [33-36]. Issues of flexure strength dependence on surface condition are likely to be more relevant as armor tile thicknesses decrease. Bending-induced deflections for a given load (or impact) will increase as tile thickness decreases, and if those deflections are sufficient enough to cause (tensile stress induced) failure in the ceramic tile, then proactively increasing flexure strength (e.g., performing finer grit diamond machining) in the ceramic tile will lessen the likelihood of its failure. Armor ceramic thicknesses that tend to be relatively thin (e.g., WC tiles, body armor) will probably be more affected by flexure-strengthening actions (e.g., finer surface finishes, application of passive oxidation layer on SiC ceramics, etc.) than armor ceramics that are relatively thick (e.g., thick ceramic tiles in vehicular armor).

The dependence of tile strength on surface condition may have a different degree of severity for armor ceramics that have a smaller average grain size or that are inherently stronger than CAP3 AD-995 alumina. The size of the grains comprising the majority of the volume in CAP3 AD-995 alumina are of the scale of the calculated strength-limiting flaw size per Eq. 8; that will probably not be the case for finer-grained monolithic ceramics that are stronger. Though finer grit diamond machining increased the strength of CAP3 AD-995 by up to 15% in the present study, an analogous increase in finer grit machining of a fine-grained monolithic ceramic may be more substantial and even sufficient enough to cause the dominant strength-

limiting flaw to change as a function of machining condition [37]. Such a strength dependence on machining examination is currently underway by the authors involving hot-pressed SiCs that are approximately 50% stronger than CAP3 AD-995 and have a grain size distribution whose maximum size is less than 10 μm; the effects of machining will be quantified in similar fashion to how CAP3 AD-995 was characterized in the present study.

From a manufacturing quality control perspective, the equibiaxial flexure test apparatus and method utilized in the present study may potentially be used as a "proof test" and discriminate stronger tiles from weaker ones. If stronger tiles (i.e., tiles that can withstand greater center-line deflection prior to fracturing) were linkable to better ballistic performance, then this equibiaxial flexure test could be used to filter out and eliminate from consideration those tiles that have low potential for ballistic performance.

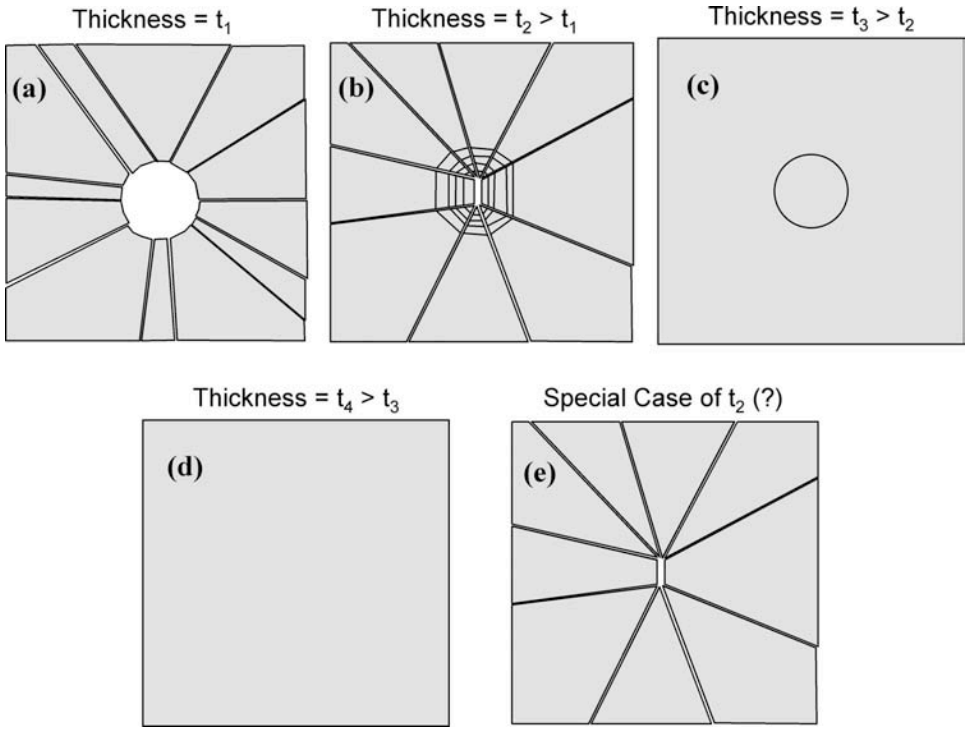

Figure 28. Schematic of fracture pattern trends due to on-center impact (as a function of tile thickness) and their proposed link to equibiaxial flexure testing. Shock stress wave effects, though affective, are not considered here. Back of the tile shown and impact direction is perpendicular to the shown faces and toward the reader.

(a) Tile thickness (t) is so thin ($t = t_1$) that the projectile completely penetrates. This is similar in appearance to an invalid equibiaxial flexure test (see Figs. 7-8). Controlled machining quality of the ceramic probably will have little or no effect.

(b) Tile is sufficiently thick ($t = t_2 > t_1$) to achieve partial penetration. Energy of threat is sufficiently high enough to cause concentric conoid patterns on previously created backface-equibiaxial-tension-induced cracks. This too is similar in appearance to an invalid equibiaxial flexure test (see Figs. 7-8). Controlled machining quality of the ceramic may have an effect and perhaps it may be able to promote fracture toward that of the pattern of $t = t_3$.

(c) Tile is sufficiently thick ($t = t_3 > t_2$) so that backface-equibiaxial-tension-induced cracks are not created; however energy of the threat is sufficient to only drive a single conoid crack through to the backface. Controlled machining quality of the ceramic probably will have little or no effect on this.

(d) Tile is thick enough ("semi-infinite", $t = t_4 > t_3$) that no cracks are created on the back face. Controlled machining quality of the ceramic probably will have little or no effect on this.

(e) Special case of $t = t_2$: partial penetration was achieved, and the energy of the threat was not sufficient to drive conical cracks through to its surface. Fracture pattern the same as that from valid equibiaxial flexure testings (see Figs. 7-8).

4. Conclusions

The effect of surface condition on the uniaxial and equibiaxial flexure strength of CoorsTek's CAP3 AD-995 alumina was examined. The following four surface conditions were considered: as-fired (i.e., unmachined) surfaces; the surface condition produced by CoorsTek's standard surface grinding procedures (i.e., the surface condition they will produce on tiles unless otherwise specified); the surface condition resulting from uniaxial surface grinding with 320-grit diamond machining (i.e., that surface machining method specified for ASTM C1161 ceramic flexure bars), and rotary surface grinding with 320-grit diamond machining.

CoorsTek manufactures and markets two grades of compositionally equivalent, 99.5%-purity alumina, designated by CoorsTek as AD-995 and CAP3 AD-995; the latter was tested in the present study. CoorsTek reports the same average grain size for these two 99.5% grades (an average size of 1.5 and 5.7 μm was respectively measured for AD-995 and CAP3 AD-995 in the present study is in conflict with that); though those values may be statistically correct in their measurements, the narrow and wide grain size distributions that the AD-995 and CAP3 AD-995 grades respectively have are not illustrated by that mean value. It is in the investigator's interest to understand the grain size distribution of the 99.5%-purity they are testing and to recognize which of the two grades that they are actually interrogating. If that information is not respected, and results have differences with those from other studies involving 99.5%-purity aluminas, then the possible (and potentially simple) explanation for those differences may be lost.

Strength depended on surface condition. Surfaces that were uniaxial or rotary ground using 320-grit diamond machining generated the highest strengths (equibiaxial flexure characteristic strength = 280 MPa) CAP3 AD-995 alumina, followed in descending order of strengths from as-fired surfaces (equibiaxial flexure characteristic strength = 264 MPa), and then strengths from surfaces produced by CoorsTek's standard grinding procedure (equibiaxial flexure characteristic strength = 244 MPa). Those differences in strengths are statistically significant with 95% confidence. These results show that finer surface finishes produced by 320-grit machining can increase flexure strength, and suggest that CoorsTek's standard surface grinding procedure of CAP3 AD-995 tiles is perhaps too aggressive.

The balance of the extra cost of machining CAP3 AD-995 alumina and their effects on strength is subjective. Though CoorsTek's "standard" machining will provide a tile whose dimensions will have stricter tolerances than those of "as-fired" tiles for an extra cost of

$14/tile (4x4x0.118" tile geometry), that comes at the expense of lower strengths - a 7-8% decrease. The characteristic strengths of 320-grit machined tiles were 6% and 15% greater than for tiles with as-fired surfaces and CoorsTek "standard" ground surfaces, respectively, but that resulted from an additional expense of $45/tile. If desire remains to have CoorsTek perform the surface machining of their CAP3-AD995 alumina tiles, then a requested combination of a less aggressive machining practice and a finer grit grinding wheel should be considered by the customer if strength retention is deemed important. Clearly, the 320-grit machining benefits strength; however, justification of the extra expense for that relatively low amount of strengthening will probably need to be made on a case by case basis.

As expected, chamfered edges were observed to have a beneficial effect on uniaxial flexure strength. *Not* chamfering uniaxial flexure specimens resulted in a strength loss of approximately 4-8% for a given machining condition for CAP3 AD-995 alumina. The reduction in strength correlated with failure consistently being initiated at the edge of these specimens (an occurrence not observed when bend bar edges were chamfered). A lack of edge chamfering inherently had no effect on equibiaxial flexure strength; however, it may as a tile is mechanically loaded closer to one of its edges (and that edge is chamfered or unchamferred). Chamfering edges in ceramic specimens and components has been long recognized to increase strength; however, in spite of that recognized effect, the study of chamfered or unchamferred edges in the present study was revisited because ceramic tiles are often purchased with unchamferred edges and interest existed to statistically illustrate their effect on strength.

Uniaxial flexure testing with ASTM C1161B produced strengths that were susceptible to machining direction, whereas equibiaxial flexure strengths were not. The directional-dependence on uniaxial flexure strength was a consequence of the interaction between the extent of anistropic machining damage and the relatively large average grain size of CAP3 AD-995 alumina. The directional-dependence on uniaxial flexure strength effect only complicates the general interpretation of flexure strength's dependence on surface condition, whereas equibiaxial flexure testing facilitates surface condition comparisons because of its "averaging effect" on machining directionality - it is perhaps a better flexure test for assessing flexure strength of armor tiles.

Equibiaxial flexure strengths were ~ 20% less than uniaxial flexure strengths for any of the four investigated surface conditions: this amount correlates very well with predicted strength-

size-scaling between the two geometries using Weibull theory. Because this failure stress is lower, and probably more representative of on-center ballistic loading of ceramic tiles, its use is desirably conservative and perhaps better suited as input in ballistic models that consider such deflections.

The results from this study show that machining practices can be employed to increase flexure strength which can potentially have beneficial ramifications on ballistic performance when tile thickness is influential (i.e., relatively thin). Issues of flexure strength dependence on surface condition are likely to be more relevant as armor tile thicknesses decrease. Bending-induced deflections for a given load (or impact) will increase as tile thickness decreases, and if those deflections are sufficient to cause (tensile stress induced) failure in the ceramic tile, then proactively increasing flexure strength (e.g., performing finer grit diamond machining) in the ceramic tile will lessen the likelihood of its failure. Tile thicknesses that tend to be relatively thin (e.g., WC tiles, body armor) will probably be more affected by flexure-strengthening actions (e.g., finer surface finishes, application of passive oxidation layer on SiC ceramics, etc.) than tiles that are relatively thick (e.g., thick ceramic tiles in vehicular armor).

5. Acknowledgements

This research was supported in part by an appointment to the Research Participation Program at the U.S. Army Research Laboratory administered by the Oak Ridge Institute for Science and Education through an interagency agreement between the U.S. Department of Energy and USARL.

Gratitude is expressed for some of the SEM imaging performed by ORNL's H. -T. Lin, the coordination of the fixturing machining performed by ORNL's J. E. Shelton and M. K. Ferber, and the piezoluminescence characterization performed by ORNL's M. J. Lance. The authors too wish to thank NIST's G. D. Quinn for his comments and input. Lastly, C. Hoppel, S. Ghiorse, S. McSpadden, and M. Radovic are thanked for reviewing the manuscript and for their useful comments.

6. References

[1] "Standard Test Method for Flexure Strength of Advanced Ceramics at Ambient Temperatures," ASTM C1161-94, Annual Book of ASTM Standards, Vol. 15.01, American Society for Testing and Materials, West Conshohocken, PA, 2001.

[2] "Plate: Aluminum Oxide Ceramic (For Use in Armor Composites)," MIL-P-46199 (MR), June 1989.

[3] "Armor Products," CoorsTek, www.coorstek.com, 2001.

[4] "Material Properties Standard 2000," CoorsTek, www.coorstek.com, 2001.

[5] "Standard Test Method for Dynamic Young's Modulus, Shear Modulus, and Poisson's Ratio for Advanced Ceramics by Impulse Excitation of Vibration," ASTM C1259, Annual Book of ASTM Standards, Vol. 15.01, American Society for Testing and Materials, West Conshohocken, PA, 2002.

[6] "Standard Practice for Measuring Ultrasonic Velocity in Materials," ASTM E494, Annual Book of ASTM Standards, Vol. 3.03, American Society for Testing and Materials, West Conshohocken, PA, 2000.

[7] J. Foster, CoorsTek, personal conversation, October 2000.

[8] J. E. Ritter, Jr., K. Jakus, A. Batakis, and N. Bandyopadhyay, "Appraisal of Biaxial Strength Testing," Journal of Non-Crystalline Solids, **38-39** 419-24 (1980).

[9] J. S. Wallace, E. R. Fuller, Jr., and S. W. Freiman, "Mechanical Properties of Aluminum Nitride Substrates," Report NISTIR 5903, U.S. Department of Commerce, 1996.

[10] A. A. Wereszczak, T. P. Kirkland, K. Breder, H. -T. Lin, and M. J. Andrews, "Biaxial Strength, Strength-Size-Scaling, and Fatigue Resistance of Alumina and Aluminum Nitride Substrates," *International Journal of Microcircuits and Electronic Packaging*, **22** 446-458 (1999).

[11] "Standard Test Method for Biaxial Flexure Strength (Modulus of Rupture) of Ceramic Substrates," ASTM F394, Annual Book of ASTM Standards, Vol. 10.04, American Society for Testing and Materials, West Conshohocken, PA, 1998.

[12] S. J. Cimpoeru, "The Durability Aspects of Armouring With Ceramic Tiles," *Journal of Materials Science Letters*, **15** 837-39 (1996).

[13] "Standard Test Method for Monotonic Equibiaxial Flexural Strength of Advanced Ceramics at Ambient Temperature," ASTM C1499, Annual Book of ASTM Standards, Vol. 15.01, American Society for Testing and Materials, West Conshohocken, PA, in press, 2002.

[14] "Standard Test Method for Monotonic Equibiaxial Flexural Strength of Advanced Ceramics at Ambient Temperatures," ASTM C1499, Annual Book of ASTM Standards, Vol. 15.01, American Society for Testing and Materials, West Conshohocken, PA, 2001.

[15] F. F. Vitman and V. P. Pukh, "A Method for Determining the Strength of Sheet Glass," *Aavodskaya Laboratoriya*, **29** 863-67 (1963).

[16] "Determination of Bending Strength," Duetsches Institut fur Normung, **52** 292 (1984).

[17] "Practice for Reporting Uniaxial Strength Data and Estimating Weibull Distribution Parameters for Advanced Ceramics," ASTM C1239, Annual Book of ASTM Standards, Vol. 15.01, American Society for Testing and Materials, West Conshohocken, PA, 2001.

[18] "Life Prediction Methodology for Ceramic Components of Advanced Heat Engines, Phase 1, Prepared by AlliedSignal Engines, Phoenix, AZ, ORNL/Sub/89-SC674/1-2, DOE Office of Transportation Technologies, 1995.

[19] "Standard Practice for Fractography and Characterization of Fracture Origins in Advanced Ceramics," ASTM C1322, Annual Book of ASTM Standards, Vol. 15.01, American Society for Testing and Materials, West Conshohocken, PA, 2001.

[20] N. A. Weil and I. M. Daniel, "Analysis of Failure Probabilities in Nonuniformly Stressed Brittle Materials," *Journal of the American Ceramic Society*, **47** 268-74 (1964).

[21] S. B. Batdorf, "Some Approximate Treatments of Fracture Statistics for Polyaxial Tension," *International Journal of Fracture*, **13** 5-11 (1977).

[22] K. Breder, T. Andersson, and K. Schölin, "Fracture Strength of _- and _-SiAlON Measured by Biaxial and Four-Point Bending," *Journal of the American Ceramic Society*, **73** 2128-30 (1990).

[23] "Standard Test Method for Flexural Strength (Modulus of Rupture) of Electronic Grade Ceramics," ASTM F417, Annual Book of ASTM Standards, Vol. 10.04, American Society for Testing and Materials, West Conshohocken, PA, 1998.

[24] R. W. Rice, J. J. Mecholsky, Jr., and P. F. Becher, "The Effect of Grinding Direction on Flaw Character and Strength of Single Crystal and Polycrystalline Ceramics," *Journal of Materials Science*, **16** 853-862 (1981).

[25] J. A. Salem, N. N. Nemeth, L. M. Powers, and S. R. Choi, "Reliability Analysis of Uniaxially Ground Brittle Materials, *Journal of Engineering for Gas Turbines and Power*, **118** 863-71 (1996).

[26] A. A. Wereszczak, T. P. Kirkland, and H. -T. Lin, and S. K. Lee, "Intermediate Temperature Inert Strength and Dynamic Fatigue of Candidate Silicon Nitrides for Diesel Exhaust Valves," *Ceramic Engineering and Science Proceedings*, **21** 497-508 (2000).

[27] A. A. Wereszczak, H. -T. Lin, T. P. Kirkland, M. J. Andrews, and S. K. Lee, "Strength and Dynamic Fatigue of Silicon Nitride at Intermediate Temperatures," in review, *Journal of Materials Science*, (2001).

[28] R. W. Rice, "Correlation of Machining-Grain-Size Effects on Tensile Strength with Tensile Strength-Grain-Size Behavior," *Journal of the American Ceramic Society*, **76** 1068-70 (1993).

[29] R. W. Rice, "Effects of Ceramic Microstructural Character on Machining Direction – Strength Anisotropy," pp. 185-204 in *Machining of Advanced Materials, NIST Special Publication 847*, Ed. S. Jahanmir, US Department of Commerce, 1993.

[30] H. G. Wobker and H. K. Tonshoff, "High Efficiency Grinding of Structural Ceramics," pp. 171-183 in *Machining of Advanced Materials, NIST Special Publication 847*, Ed. S. Jahanmir, US Department of Commerce, 1993.

[31] S. -J. Cho, K. -J. Yoon, J. -J. Kim, and K. -H. Kim, "Influence of Humidity on the Flexural Strength of Alumina," *Journal of the European Ceramic Society*, **20** 761-764 (2000).

[32] S. -J. Cho, K. -J. Yoon, J. -J. Kim, and Y. -K. Cho, "Effects of Environmental Temperature and Humidity on the Flexural Strength of Alumina and Measurement of Inert Strength," unpublished results.

[33] D. A. Shockey, D. J. Rowcliffe, K. C. Dao, and L. Seaman, "Particle Impact Damage in Silicon Nitride," *Journal of the American Ceramic Society*, **73** 1613-19 (1990).

[34] D. Sherman and D. G. Brandon, "The Ballistic Failure Mechanisms and Sequence in Semi-Infinite Supported Alumina Tiles," *Journal of Materials Research*, **12** 1335-1343 (1997).

[35] D. Sherman and T. Ben-Shushan, "Quasi-Static Impact Damage in Confined Ceramic Tiles," *Internal Journal of Impact Engineering*, **21** 245-265 (1998).

[36] D. Sherman, "Impact Failure Mechanisms in Alumina Tiles on Finite Thickness Support and the Effect of Confinement," *Internal Journal of Impact Engineering*, **24** 313-328 (2000).

[37] A. A. Wereszczak, A. S. Barnes, K. Breder, and S. Binapal, "Probabilistic Strength of {111} n-Type Silicon," *Journal of Materials Science: Materials in Electronics*, **11** 291-303 (2000).

Appendix A

Failure Stress Values of all Uniaxial Flexure Specimens

As-Fired Chamferred	As-Received Chamferred	Longitudinal Chamferred	Transverse Chamferred	Rotational Chamferred	As-Fired Unchamferred	As-Received Unchamferred	Rotational Unchamferred
Unaxial Flexure Failure Stress (MPa)	Unaxial Flexure Failure Stress (MPa)	Unaxial Flexure Failure Stress (MPa)	Unaxial Flexure Failure Stress (MPa)	Unaxial Flexure Failure Stress (MPa)	Unaxial Flexure Failure Stress (MPa)	Unaxial Flexure Failure Stress (MPa)	Unaxial Flexure Failure Stress (MPa)
274.1	172.4	248.4	299.4	290.5	231.5	244.4	285.5
289.3	260.5	287.5	312.5	301.2	252.0	250.2	297.9
292.8	272.6	290.8	328.9	307.3	252.9	257.3	308.3
294.5	277.1	301.4	330.0	321.8	264.8	258.8	317.0
294.6	277.8	305.4	333.7	322.6	274.6	261.6	317.7
301.6	281.0	308.9	334.4	346.0	275.2	264.4	318.1
302.6	281.3	313.3	335.2	347.9	278.9	264.7	319.0
308.1	281.3	316.6	336.6	350.2	281.9	270.3	320.3
309.8	282.3	317.4	338.6	352.0	284.9	272.8	332.3
311.5	286.3	319.4	341.0	359.0	285.0	274.0	332.5
316.3	287.0	319.4	342.2	360.4	286.7	275.1	334.7
319.9	287.3	325.5	343.5	361.6	290.3	277.2	336.3
322.5	288.5	325.7	344.1	365.4	292.3	277.6	340.8
322.8	290.7	327.4	344.1	368.3	295.8	278.5	342.7
324.9	290.9	329.8	344.2	368.5	298.2	279.6	342.9
328.0	292.2	329.9	345.8	372.3	300.3	279.9	343.1
331.8	293.3	331.8	347.1	374.0	302.2	280.2	343.2
333.9	293.5	332.3	347.4	375.3	304.3	280.7	343.7
334.0	294.0	334.8	347.6	377.4	312.2	282.3	344.0
334.6	295.6	336.0	347.9	377.9	314.6	282.6	345.0
335.5	296.0	336.4	348.5	381.7	315.4	284.1	346.3
338.3	298.9	337.7	349.9	382.1	315.7	284.7	348.7
341.3	300.9	338.3	351.5	383.1	319.8	287.3	349.1
344.0	302.0	341.3	352.1	385.2	320.4	287.6	354.3
345.0	303.0	344.9	356.0	388.3	322.4	288.3	355.0
346.5	303.9	346.4	357.0	391.2	327.4	289.2	359.6
349.1	304.3	353.3	357.8	392.7	329.5	291.7	361.4
354.2	304.4	353.5	365.6		333.4	292.9	
357.9	305.6				340.2	294.5	
367.5	305.7				341.8	299.1	

Appendix B

Failure Stress Values of all Equibiaxial Flexure Specimens

As-Fired	As-Received	Transverse (or Long)	Rotational
Equibiaxial Failure Stress (MPa)	Equibiaxial Failure Stress (MPa)	Equibiaxial Failure Stress (MPa)	Equibiaxial Failure Stress (MPa)
231.7	227.7	252.1	248.3
233.8	237.9	265.9	260.6
241.4	240.0	268.5	261.2
246.8	243.1	277.4	282.6
251.5	246.6	287.9	287.6
252.6	251.1	289.0	293.6
260.0			
260.1			
262.4			
272.6			
273.0			
275.9			
280.2			

NO. OF COPIES	ORGANIZATION
2	DEFENSE TECHNICAL INFORMATION CENTER DTIC OCA 8725 JOHN J KINGMAN RD STE 0944 FT BELVOIR VA 220060-6218
1	HQDA DAMO FDT 400 ARMY PENTAGON WASHINGTON DC 20310-0460
1	OSD OUSD(A&T)/ODDR&E(R) DR R J TREW 3800 DEFENSE PENTAGON WASHINGTON DC 20301-3800
1	COMMANDING GENERAL US ARMY MATERIEL CMD AMCRDA TF 5001 EISENHOWER AVE ALEXANDRIA VA 22333-0001
1	INST FOR ADVNCD TCHNLGY THE UNIV OF TEXAS AT AUSTIN 3925 W BRAKER LN STE 400 AUSTIN TX 78759-5316
1	DARPA SPECIAL PROJECTS OFFICE J CARLINI 3701 N FAIRFAX DR ARLINGTON VA 22203-1714
1	US MILITARY ACADEMY MATH SCI CTR EXCELLENCE MADN MATH THAYER HALL WEST POINT NY 10996-1786
1	DIRECTOR US ARMY RESEARCH LAB AMSRL CI AI R 2800 POWDER MILL RD ADELPHI MD 20783-1197
3	DIRECTOR US ARMY RESEARCH LAB AMSRL CI LL 2800 POWDER MILL RD ADELPHI MD 20783-1197
3	DIRECTOR US ARMY RESEARCH LAB AMSRL CI IS T 2800 POWDER MILL RD ADELPHI MD 20783-1197
	ABERDEEN PROVING GROUND
4	DIR USARL AMSRL CI LP (BLDG 305)

NO. OF COPIES	ORGANIZATION
1	CERADYNE D PUCKETT 3169 REDHILL AVE COSTA MESA CA 92626
1	CERCOM R PALICKA 1960 WATSON WAY VISTA CA 92083
2	COMMANDER US ARMY TACOM AMSTA JSK L FRANKS D TEMPLETON WARREN MI 48397-5000
1	CONNECTICUT RESERVE TECH S DUFFY 2400 SUPERIOR AVE #208 CLEVELAND OH 44114
1	COORSTEK B SEEGMILLER 600 9TH ST GOLDEN CO 80401
1	NATIONAL INST OF STDS & TECH G QUINN BLDG 223 RM A256 100 BUREAU DRIVE STOP 8520 GAITHERSBURG MD 20899-8520
1	NASA-GRC J SALEM MS-49-7 21000 BROOKPARK RD CLEVELAND OH 44135

1 NETWORK COMPUTING SERVICES
T HOLMQUIST
1200 WASHINGTON AVE S
MINNEAPOLIS MN 55415

1 NGIC
IANG GS MT MS 306
J CRIDER
2055 BOULDERS RD
CHARLOTTESVILLE VA
22911-8318

20 OAK RIDGE NATIONAL LAB
A WERESZCZAK
PO BOX 2008
BLDG 4515 MS 6068
OAK RIDGE TN 37831-6068

1 RUTGERS, STATE UNIV OF NJ
D NIESZ
CENTER FOR CERAMIC RSCH
607 TAYLOR RD
PISCATAWAY NJ 08854-8065

1 SAINT GOBAIN ABRASIVES
K BREDER
HIGGINS GRINDING TECH CTR
1 NEW BOND ST MS 413-201
WORCESTER, MA 01615-0008

1 SAINT GOBAIN/CARBORUNDUM
J RUPPEL
23 ACHESON DR
NIAGARA FALLS NY 14303

2 SAINT GOBAIN IND CERAMICS
R LICHT
V PUJARI
1 GODDARD RD
NORTHBORO MA 01532-1545

1 SIMULA
10016 S 51ST ST
PHOENIX AZ 85044

1 UNIV OF DAYTON RSCH INST
R WILLS
CERAMIC AND GLASS LABS
300 COLLEGE PARK
DAYTON OH 45469-0182

7 US ARMY RESEARCH OFC
A CROWSON
B LAMATTINA
W MULLINS
J PRATER
A RAJENDRA
E SEGAN
D STEPP
PO BOX 12211
RESEARCH TRIANGLE PARK NC
27709-2211

1 USA SBCCOM
SOLDIER SYSTEMS CENTER
AMSSB RCP SS
KANSAS ST
NATICK MA 01760-5019

NO. OF COPIES	ORGANIZATION
	ABERDEEN PROVING GROUND
?	DIR USARL
	AMSRL CS IO FI
	M ADAMSON
	AMSRL WM
	J SMITH
	AMSRL WM B
	A HORST
	AMSRL WM M
	B FINK
	J MCCAULEY
	AMSRL WM MA
	S MCKNIGHT
	AMSRL WM MB
	L BURTON
	R CARTER
	P DEHMER
	G GAZONAS
	S GHIORSE
	C HOPPEL
	AMSRL WM MC
	J ADAMS
	J BEATTY
	E CHIN
	K DOHERTY
	J LASALVIA
	J SWAB (10 CPS)
	AMSRL WM MD
	W ROY
	AMSRL WM T
	B BURNS
	M ZOLTOSKI
	AMSRL WM TA
	W BRUCHEY
	W GOOCH
	T HAVEL
	E HORWATH
	M NORMANDIA
	AMSRL WM TC
	R COATES
	AMSRL WM TD
	T HADUCH
	T MOYNIHAN
	N RUPERT
	S SCHOENFELD